Dalton Transactions

Accepted Manuscript

ROYAL SOCIETY OF CHEMISTRY

www.rsc.org/dalton

Switching from Antiferromagnetic to Ferromagnetic Coupling in Heptanuclear $[M^t_6M^c]^{n+}$ Complexes by Going from an Achiral to a Chiral Triplesalen Ligand

Chandan Mukherjee,[a,b] Veronika Hoeke,[a] Anja Stammler,[a] Hartmut Bögge,[a] Jürgen Schnack,[c] and Thorsten Glaser*[,a]

[a] *Lehrstuhl für Anorganische Chemie I, Fakultät für Chemie, Universität Bielefeld, Universitätsstr. 25, D-33615 Bielefeld, Germany*

[b] *New address: Department of Chemistry, Indian Institute of Technology Guwahati, Guwahati-781039, Assam, India*

[c] *Fakultät für Physik, Universität Bielefeld, Universitätsstr. 25, D-33615 Bielefeld, Germany*

* To whom correspondence should be addressed. E-mail: thorsten.glaser@uni-bielefeld.de; Fax: +49-521-106-6003

Abstract

The chiral triplesalen ligand H_6chand^{RR} has been used to synthesize the chiral heptanuclear complexes $[\{(chand^{RR})Mn^{III}_3\}_2\{Fe^{II}(CN)_6\}](ClO_4)_2$ (^{RR}**[Mn$^{III}_6$Fe^{II}]**$(ClO_4)_2$) and $[\{(chand^{RR})Fe^{III}_3\}_2\{Fe^{II}(CN)_6\}](ClO_4)_2$ (^{RR}**[Fe$^{III}_6$Fe^{II}]**$(ClO_4)_2$), which have been characterized by single-crystal X-ray diffraction, mass spectrometry, elemental analysis, FT-IR, Mössbauer, and UV-vis spectroscopies, electrochemistry, as well as DC and AC magnetic susceptibility measurements. The half-wave potential of the Fe^{III}/Fe^{II} couple in ^{RR}**[Mn$^{III}_6$Fe^{II}]$^{2+}$** and ^{RR}**[Fe$^{III}_6$Fe^{II}]$^{2+}$** is $E_{1/2}$ = +0.21 and +0.75 V vs Fc^+/Fc, respectively, which (*i*) corresponds to a strong stabilization of the reduced Fe^{II} species compared to

the redox couple of free $[Fe^{II/III}(CN)_6]^{4-/3-}$ and (*ii*) indicates a significant difference of the electronic coupling with the $\{(chand^{RR})M^t\}^{3+}$ units (M^t = Mn^{III}, Fe^{III}). Analysis of the DC magnetic data (μ_{eff} vs T, VTVH) of both complexes by a full-matrix diagonalization of the spin-Hamiltonian including isotropic exchange, zero-field splitting with full consideration of the relative orientation of the **D** tensors and Zeeman interactions reveals ferromagnetic interactions of $J_{Mn\text{-}Mn}$ = +0.17 ± 0.02 cm^{-1} for $^{RR}[Mn^{III}_6Fe^{II}]^{2+}$ with D_{Mn} = -3.4 ± 0.3 cm^{-1} and $J_{Fe\text{-}Fe}$ = +0.235 ± 0.005 cm^{-1} with D_{Fe} = 0 for $[Fe^{III}_6Fe^{II}]^{2+}$. The comparison of the molecular structures of $^{RR}[Mn^{III}_6Fe^{II}]^{2+}$ and $^{RR}[Fe^{III}_6Fe^{II}]^{2+}$ to those of the heptanuclear complexes $[M^t_6M^c]^{n+}$ using the achiral triplesalen ligand $(talen^{t\text{-}Bu_2})^{6-}$ reveals significant differences in the ligand folding, smaller C-C bond distances in the central phloroglucinol ring and larger HOMA values. This indicates more aromatic character and less heteroradialene contribution in $^{RR}[Mn^{III}_6Fe^{II}]^{2+}$ and $^{RR}[Fe^{III}_6Fe^{II}]^{2+}$, which explains the switching from antiferromagnetic coupling in $[M^t_6M^c]^{n+}$ to ferromagnetic coupling in $^{RR}[M^t_6M^c]^{n+}$ by a stronger contribution of the spin-polarization mechanism. This establishes a magnetostructural correlation between the structural parameters describing the aromaticity of the central phloroglucinol unit and the observed exchange couplings $J_{Mn\text{-}Mn}$.

Introduction

Since the discovery of the single-molecule magnet (SMM) behavior of Mn_{12} in 1993,[1] strong efforts have been devoted to the study of the magnetic properties of SMMs,[2] to the understanding of their basic physics,[3] to the synthesis of improved SMMs,[4] and to their applications.[5] SMMs exhibit a slow relaxation of the magnetization at low temperatures due to an energy barrier *U* for spin reversal. For a complex of given spin ground state S_t and zero-field splitting D_{S_t}, the energy barrier is given by $U = D_{S_t} \cdot S_t^2$ (or $U = D_{S_t} \cdot (S_t^2$ -

1/4) for half-integer spin ground states S_t). There are two mechanisms to overcome this energy barrier: (*i*) a thermal pathway over the top of the barrier and (*ii*) a tunneling pathway through the barrier. Besides other effects introducing a transversal field component, the probability for the quantum mechanical magnetization tunneling p is related to $p \propto 1 - \exp(E_{S_t}/D_{S_t})^{S_t}$ with E_{S_t}/D_{S_t} being the rhombicity.[6] The latter is zero for molecules with at least a C_3 axis. Thus, a rational approach to new SMMs must include these three necessary requirements: (*i*) a high-spin ground state S_t, which decreases both the thermal and the tunneling relaxation, (*ii*) a strong negative zero-field splitting D_{S_t}, and (*iii*) a control of the molecular topology to enforce a symmetry of at least C_3.

In order to establish a recipe to ensure high spin ground states S_t by ferromagnetic interactions, we have started a program[7] to utilize the spin-polarization mechanism[8] that is well established in organic chemistry.[9] E. g., the *meta*-phenylene bridging unit is a robust ferromagnetic coupling unit. In this respect, we have successfully employed 1,3,5-trihydroxybenzene **A** (phloroglucinol)[10] as a ferromagnetic coupling unit between three Cu^{II} ions.[7a] As this bridging unit already possesses C_3 symmetry, we only needed to add a source for magnetic anisotropy, which was done by introducing a salen-like coordination environment (**B**).[11] This resulted in the ligand triplesalen **C** (Scheme 1).[7b,12] Trinuclear triplesalen Cu^{II}_3 complexes exhibit indeed ferromagnetic interactions.[13] Moreover, irrespective of the metal ions, the trinuclear complexes $[(talen^{t\text{-}Bu_2})M_3]^{n+}$ of the substituted triplesalen ligand $H_6talen^{t\text{-}Bu_2}$ (Scheme 1) exhibit a certain degree of ligand folding, with all three terminal 'metal-phenolate units' bending to the same site with respect to the central phloroglucinol plane.[13b,14] This results in an overall bowl-shaped molecular structure, which pre-organizes the three metal ions for binding to three nitrogen atoms of a hexacyanometallate in a facial fashion.[15] In this way, two trinuclear triplesalen complexes $[(talen^{t\text{-}Bu_2})M_3]^{n+}$ are able to encapsulate a hexacyanometallate in a

supramolecular assembly to heptanuclear $\mathbf{[M^t_6M^c]^{n+}}$ (=$[\{(talen^{t\text{-}Bu_2})M^t_3\}_2\{M^c(CN)_6\}]^{n+}$) complexes by molecular recognition. The strong driving force for this assembly allows the synthesis of several heptanuclear complexes: $\mathbf{[Mn^{III}_6Cr^{III}]^{3+}}$,[16] $\mathbf{[Mn^{III}_6Fe^{III}]^{3+}}$,[17] $\mathbf{[Mn^{III}_6Fe^{II}]^{2+}}$,[17b] $\mathbf{[Mn^{III}_6Co^{III}]^{3+}}$,[18] $\mathbf{[Mn^{III}_6Os^{III}]^{3+}}$,[19] $\mathbf{[Mn^{III}_6Os^{II}]^{2+}}$,[19] and $\mathbf{[Mn^{III}_6Mn^{III}]^{3+}}$.[20] $\mathbf{[Mn^{III}_6Cr^{III}]^{3+}}$ is an SMM with anisotropy barriers up to 28 K depending on the counterions and on the solvate,[16b] while $\mathbf{[Mn^{III}_6Mn^{III}]^{3+}}$ is an SMM with a record hysteretic opening up to ± 10 T.[20b] However, despite our efforts to follow a rational approach, the blocking temperatures of these SMMs do not exceed 2 K due to the moderate heights of their anisotropy barriers U^{eff}.

We have analyzed the magnetic properties of all $\mathbf{[M^t_6M^c]^{n+}}$ complexes with the appropriate spin-Hamiltonian including HDvV exchange, Zeeman-effect, zero-field splitting, and the relative orientations of the zero-field splitting tensors. Surprisingly, the coupling between the Mn^{III} ions in the trinuclear Mn^{III}_3 triplesalen subunits[16,17,18,19,20,21] turned out to be slightly antiferromagnetic in the range of $-1.2 \le J \le -0.2$ cm^{-1} despite the envisioned ferromagnetic interactions by the phloroglucinol coupling unit (as observed in the Cu^{II}_3 complexes). We have analyzed the molecular and electronic structures of our extended phloroglucinol ligands and complexes and established by NMR, IR, and electronic absorption spectroscopies as well as by analysis of high-resolution molecular structures that the ligands have to be described as the N-protonated tautomer **E** with a non-aromatic heteroradialene electronic structure instead of the anticipated O-protonated aromatic tautomer **D** (Scheme 2).[9c,13c,13e,13f,22] This heteroradialene structure is also prevalent in the complexes. As the spin-polarization mechanism requires a delocalized aromatic central π-system, the heteroradialene formation prevents an efficient spin-polarization mechanism and is thus responsible for the occurrence of the observed antiferromagnetic interactions.[9c]

Here, we present the application of the chiral triplesalen ligand H_6chand^{RR} (Scheme 1) for the synthesis of analogous heptanuclear complexes. This ligand and its enantiomer H_6chand^{SS} were initially synthesized based on the success of metal complexes of chiral salen ligands in enantioselective catalysis. In this respect, we have employed $[(chand^{RR})\{Mn^{III}Cl\}_3]$ and $[(chand^{SS})\{Mn^{III}Cl\}_3]$ in the enantioselective epoxidation of olefins[21b] and $[(chand^{RR})\{Fe^{III}Cl\}_3]$ in the enantioselective sulfoxidation of thioethers.[22a] Their molecular structures differ from those of the $H_6talen^{t\text{-}Bu_2}$ complexes in that the terminal phenolate rings and the central phloroglucinol ring are bent to opposite sites with respect to the MN_2O_2 coordination plane, which results in a molecular structure that might be described as 'soup plate-shaped'.

The reaction of $[(chand^{RR})\{Mn^{III}(solv)_n\}_3]^{3+}$ and $[(chand^{RR})\{Fe^{III}(solv)_n\}_3]^{3+}$ with $[Fe^{III}(CN)_6]^{3-}$ directly results in the formation of the heptanuclear complexes $[\{(chand^{RR})Mn^{III}{}_3\}_2\{Fe^{II}(CN)_6\}]^{2+}$ (^{RR}**[Mn$^{III}_6$Fe^{II}]$^{2+}$**) and $[\{(chand^{RR})Fe^{III}{}_3\}_2\{Fe^{II}(CN)_6\}]^{2+}$ (^{RR}**[Fe$^{III}_6$Fe^{II}]$^{2+}$**) with unprecedented C_2-symmetric structures. ^{RR}**[Fe$^{III}_6$Fe^{II}]$^{2+}$** represents the first heptanuclear triplesalen complex not bearing terminal Mn^{III} ions. Unexpectedly, both complexes exhibit ferromagnetic interactions within the trinuclear subunits, and ^{RR}**[Mn$^{III}_6$Fe^{II}]$^{2+}$** even shows a slow relaxation of the magnetization indicative of SMM behavior. The structural changes by going from **[M$^t_6$M^c]$^{n+}$** to ^{RR}**[M^{t}Fe^{II}]$^{2+}$** are analyzed in detail and related to the exchange interactions. A magneto-structural correlation for the change of the sign of exchange coupling is presented.

Experimental Section

Materials. All reagents were obtained from commercial sources and used as supplied, unless otherwise noted. The synthesis of 2,4,6-tris{1-[(1R,2R)-2-(3,5-di-*tert*-butylsalicylaldimino)cyclohexylimino]ethyl}-1,3,5-trihydroxybenzene (H_6chand^{RR}) was reported previously.[21b]

Preparation of [{(chand^{RR})Mn$^{III}_3$($C_4H_8O_2$)$_{2.5}$}$_2${Fe^{II}($CN)_6$}]($ClO_4)_2$•2$C_4H_8O_2$•2H_2O, 1a. A solution of H_6chand^{RR} (333 mg, 0.280 mmol), $Mn(ClO_4)_2$•6H_2O (345 mg, 0.953 mmol), and Et_3N (0.15 mL, 1.1 mmol) was heated to reflux in MeOH (30 mL) for 20 min. The resulting dark-brown solution was cooled to room temperature and treated with a solution of $K_3[Fe(CN)_6]$ (46 mg, 0.140 mmol) and 18-crown-6 (188 mg, 0.711 mmol) in MeOH (5 mL). The reaction mixture was stirred at room temperature for 10 min and filtered using filter paper for extremely fine precipitates. Addition of 1,4-dioxane (6 mL) to the filtrate followed by slow evaporation of solvent caused the deposition of dark-brown crystals (**1**) suitable for single-crystal x-ray diffraction. Crystals were filtered off, washed with 1,4-dioxane, and air-dried. Yield: 156 mg (30%). IR (KBr): $\tilde{\nu}$/cm^{-1} = 2951m, 2862m, 2041s, 1618s, 1541s, 1499s, 1437m, 1389m, 1346m, 1254s, 1207w, 1177w, 1121m, 1098m, 870w, 841w, 750w, 623w, 598w, 571w, 546w. MS-ESI (+ve, MeOH): *m/z* = 1454.7 [{(chand^{RR})Mn_3}$_2${$Fe(CN)_6$}]$^{2+}$; MALDI-TOF-MS (matrix DCTB): *m/z* = 3209.3 {[{(chand^{RR})Mn_3}$_2${$Fe(CN)_6$}]($ClO_4)_3$}$^-$. $[\alpha]^{20}_D$ = -2524.0 (± 5.0), *C* = 1.03 mg / 100 mL, MeOH. Anal. Calcd for **1a** ($C_{184}H_{264}N_{18}O_{36}Cl_2Mn_6Fe$): C 58.77, H 7.08, N 6.70. Found: C 58.85, H 6.98, N 6.36.

Preparation of [{(chand^{RR})Fe$^{III}_3$($C_4H_8O_2$)$_{1.5}$(MeOH)}$_2${Fe^{II}($CN)_6$}]($ClO_4)_2$, 2a. A solution of H_6chand^{RR} (230 mg, 0.193 mmol), $Fe(ClO_4)_3$•10H_2O (220 mg, 0.412 mmol), and Et_3N (0.08 mL, 0.6 mmol) were heated to reflux in MeOH (20 mL) for 15 min. After cooling to room temperature, the resulting deep-blue solution was treated with a solution of $K_3[Fe(CN)_6]$ (32 mg, 0.097 mmol) and 18-crown-6 (131 mg, 0.496 mmol) in methanol (5 mL). The solution mixture was further heated at reflux for a moment and then filtered at room temperature using filter paper for extremely fine precipitates. 1,4-Dioxane (10 mL) was added to the filtrate (40 mL). Slow evaporation of solvent led to the deposition of a crystalline solid, which was further recrystallized from a MeOH (50 mL)/1,4-dioxane (8 mL) mixture to give brown crystals (**2**) suitable for single-crystal X-ray diffraction. Crystals

were filtered off, washed with 1,4-dioxane, and air-dried. Yield: 140 mg (59%). IR (KBr): $\tilde{\nu}$/cm^{-1} = 2951m, 2866m, 2046s, 1622s, 1539s, 1508s, 1435m, 1391m, 1360m, 1350m, 1254s, 1240s, 1207w, 1175w, 1123s, 1109m, 1051w, 864w, 843w, 820w, 781w, 750w, 596w, 565w, 544w. MS-ESI (+ve, MeOH): *m/z* = 2912.7 [{(chand^{RR})Fe$_3$}$_2${Fe(CN)$_6$}]$^+$, 1457.1 [{(chand^{RR})Fe$_3$}$_2${Fe(CN)$_6$}]$^{2+}$; MALDI-TOF-MS (matrix DCTB): *m/z* = 2914.9 [{(chand^{RR})Fe$_3$}$_2${Fe(CN)$_6$}]$^+$, 3015.0 {[{(chand^{RR})Fe$_3$}$_2${Fe(CN)$_6$}]ClO$_4$}$^+$. [α]$^{20}_D$ = -2059.0 (± 5.0), *C* = 1.02 mg / 100 mL, MeOH. Anal. Calcd for **2a** ($C_{170}H_{236}N_{18}O_{28}Cl_2Fe_7$): C 59.33, H 6.91, N 7.32. Found: C 59.26, H 6.79, N 7.70.

X-Ray Crystallography.

Crystal data for **1**: *M* = 3900.70 g mol^{-1}, $C_{192}H_{276}Cl_2FeMn_6N_{18}O_{38}$, orthorhombic, space group *C*222$_1$, *a* = 23.1459(10), *b* = 28.1670(12), *c* = 31.7049(13) Å, *V* = 20670.0(15) Å^3, *Z* = 4, ρ = 1.253 g/cm^3, μ = 0.518 mm^{-1}, *F* (000) = 8272, crystal size = 0.30 × 0.24 × 0.19 mm^3. A total of 62676 reflections (2.37 < Θ < 25.00°) were collected of which 17687 reflections were unique (R_{int} = 0.0394). *R* = 0.0488 for 14792 reflections with $I > 2\sigma(I)$, *R* = 0.0618 for all reflections, Flack parameter = -0.011(12); max/min residual electron density 0.754 and -0.399 eÅ^{-3}.

Crystal data for **2**: *M* = 3858.12 g mol^{-1}, $C_{188}H_{276}Cl_2Fe_7N_{18}O_{38}$, orthorhombic, space group *C*222$_1$, *a* = 23.4878(16), *b* = 28.214(2), *c* = 31.304(2) Å, *V* = 20745(3) Å^3, *Z* = 4, ρ = 1.235 g/cm^3, μ = 0.573 mm^{-1}, *F* (000) = 8200, crystal size = 0.40 × 0.20 × 0.20 mm^3. A total of 220880 reflections (2.26 < Θ < 25.00°) were collected of which 18218 reflections were unique (R_{int} = 0.0423). *R* = 0.0582 for 15962 reflections with $I > 2\sigma(I)$, *R* = 0.0643 for all reflections, Flack parameter = 0.009(14); max/min residual electron density 0.870 and -0.435 eÅ^{-3}.

Crystals of **1** and **2** were removed from the mother liquor and immediately cooled to

100(2) K on a Bruker AXS Kappa ApexII diffractometer (four-circle goniometer with 4K CCD detector, Mo-Kα radiation, graphite monochromator). Empirical absorption correction using equivalent reflections with SADABS 2008/1;[23] solution and refinement with SHELXS/L.[24]

The dioxane molecules (and MeOH molecules in **2**), which complete the coordination sphere of the manganese and iron atoms could be located and refined (with distance restraints for the dioxane molecules). The thermal ellipsoids of some *t*-butyl groups (the coordinated MeOH molecule in **2**) and the perchlorate anion indicate the presence of different types of disorder, which, however, could not be resolved and refined. Some restraints for the thermal parameters were used for better convergence for these molecules.

The not coordinating solvent molecules could be partially located but were strongly disordered so that they could not be properly refined. Thus, they were removed from the coordinate set and their scattering contribution determined and removed from the data set using the "SQUEEZE"[25] routine. The results from the original refinement of these positions and from "SQUEEZE" are in good agreement: The unit cell contains four solvent dioxane molecules (and two MeOH molecules in **2**) per formula unit, which are disordered over a volume, which would allow approximately the double amount of solvent molecules to be placed there.

CCDC-962786 and 962787 contain the supplementary crystallographic data for this paper. These data can be obtained free of charge from The Cambridge Crystallographic Data Centre via www.ccdc.cam.ac.uk/data_request/cif.

Other physical measurements. Infrared spectra (400-4000 cm^{-1}) of solid samples were recorded on a Shimadzu FT-IR 8400S as KBr disks. ESI and MALDI-TOF mass spectra were recorded on a Bruker Esquire 3000 ion trap mass spectrometer and a PE

Biosystems Voyager DE mass spectrometer, respectively. Elemental analyses were carried out on a LECO CHN-932 or a HEKAtech Euro EA elemental analyzer. ^{57}Fe Mössbauer spectra were recorded on an alternating constant-acceleration spectrometer. The sample temperature was maintained constant in a bath cryostat (Wissel MBBC-HE0106). ^{57}Co/Rh was used as the radiation source. Isomer shifts were determined relative to α-iron at room temperature. UV/Vis/NIR absorption spectra of solutions were measured on a Shimadzu UV-3101PC spectrophotometer in the range 190-1200 nm at ambient temperatures. The electrochemical experiments were performed on Ar-flushed MeCN solutions containing 0.1 M $(NBu_4)PF_6$ in a classical three-electrode cell. The working electrode was a glassy carbon disk electrode, the counter electrode a platinum wire, and the reference electrode was Ag/0.01 M $AgNO_3$ MeCN. All potentials are referenced to the ferrocenium/ferrocene (Fc^+/Fc) couple used as an internal standard. The electrochemical cell was connected to a Princeton Applied Research potentiostat/galvanostat model 263A. Temperature-dependent magnetic susceptibilities were measured using a SQUID magnetometer (MPMS XL-7 EC, Quantum Design) in a static field of 1 T in the range 2-290 K. Variable-temperature variable-field (VTVH) measurements were performed at 1, 4, and 7 T in the range 2-10 K with the magnetization equidistantly sampled on a 1/*T* temperature scale. For calculations of the molar magnetic susceptibilities, χ_m, the measured susceptibilities were corrected for the underlying diamagnetism of the sample holder and the sample by using tabulated Pascal's constants. AC susceptibilities were measured in the range 1.8-5.0 K in zero static field with an AC field of 3 Oe oscillating at frequencies in the range 660-1500 Hz.

Results and Discussion

Synthesis and Characterization

The reaction of preformed solvated subunits $[(chand^{RR})\{Fe^{III}(solv)_n\}_3]^{3+}$ and $[(chand^{RR})\{Mn^{III}(solv)_n\}_3]^{3+}$ with $[Fe^{III}(CN)_6]^{3-}$ resulted in single-crystals of $[\{(chand^{RR})Mn^{III}{}_3(C_4H_8O_2)_{2.5}\}_2\{Fe^{II}(CN)_6\}](ClO_4)_2 \bullet 4C_4H_8O_2$ (**1**) and $[\{(chand^{RR})Fe^{III}{}_3(C_4H_8O_2)_{1.5}(MeOH)\}_2\{Fe^{II}(CN)_6\}](ClO_4)_2 \bullet 4C_4H_8O_2 \bullet 2MeOH$ (**2**) as evidenced by single-crystal X-ray diffraction. As in all complexes of the type $\mathbf{[M^t_6M^c]^{n+}}$, coordinated 1,4-dioxane and methanol molecules, which were found in the crystals structures of **1** and **2**, are not detected in ESI and MALDI-TOF mass spectra, indicating the weakness of the $M\text{-}O_{MeOH}$ and $M\text{-}O_{dioxane}$ bonds. The samples used for magnetic and other measurements after washing and air-drying analyzed by elemental analysis as $[\{(chand^{RR})Mn^{III}{}_3(C_4H_8O_2)_{2.5}\}_2\{Fe^{II}(CN)_6\}](ClO_4)_2 \bullet 2C_4H_8O_2 \bullet 2H_2O$ (**1a**) and $[\{(chand^{RR})Fe^{III}{}_3(C_4H_8O_2)_{1.5}(MeOH)\}_2\{Fe^{II}(CN)_6\}](ClO_4)_2$ (**2a**). This loss of non-coordinated solvent molecules of crystallization has also been shown to be typical for the $\mathbf{[M^t_6M^c]^{n+}}$ complexes.

The FT-IR spectra of **1a** and **2a** exhibit the characteristic features of the coordinated ligand $(chand^{RR})^{6-}$ observed already for $[(chand^{RR})\{Mn^{III}Cl\}_3]$ [21b] and $[(chand^{RR})\{Fe^{III}Cl\}_3]$,[22a] respectively. Additionally, **1a** and **2a** exhibit very strong ν(C≡N) stretches at 2041 and 2046 cm^{-1}, respectively. In comparison, the complexes of $(talen^{t\text{-}Bu_2})^{6-}$ $\mathbf{[Mn^{III}_6Fe^{III}]^{3+}}$ and $\mathbf{[Mn^{III}_6Fe^{II}]^{2+}}$ exhibit a weak band at 2139 cm^{-1} and a strong band at 2076 cm^{-1}, respectively.[17b] This provides clear evidence that $[Fe^{III}(CN)_6]^{3-}$ has been reduced to $[Fe^{II}(CN)_6]^{4-}$ upon incorporation in $\mathbf{^{RR}[Mn^{III}_6Fe^{II}]^{2+}}$ and $\mathbf{^{RR}[Fe^{III}_6Fe^{II}]^{2+}}$ as has already been observed in the case of $\mathbf{[Mn^{III}_6Fe^{II}](BPh_4)_2}$.[17b] This will be analyzed in more detail in the electrochemistry section. However, the significant decrease of ν(C≡N) in $\mathbf{^{RR}[Mn^{III}_6Fe^{II}]^{2+}}$ and $\mathbf{^{RR}[Fe^{III}_6Fe^{II}]^{2+}}$ compared to $\mathbf{[Mn^{III}_6Fe^{II}]^{2+}}$ is surprising. This may reflect either different electronic structures, i. e. stronger back donation into the π^*(C≡N) orbitals in the $(chand^{RR})^{6-}$ complexes, and/or significant changes in the molecular structures.

Structural Characterization

Single-crystals of **1** and **2** suited for single-crystal X-ray diffraction were obtained by slow evaporation of MeOH/1,4-dioxane solvent mixtures. Both complexes crystallize in the chiral space group $C222_1$ with one half of a heptanuclear complex in the asymmetric unit. Plots of the asymmetric unit of both complexes excluding anions and non-coordinated solvent molecules are provided in Figure 1 including the numbering schemes used (thermal ellipsoid plots are given in Figure S1). The second half of the heptanuclear complexes is generated by a crystallographic C_2 axis that passes through the central Fe atom of the hexacyanoferrate and bisects the angle N41-Fe1/4-N41' of two coordinated cyanide groups. Selected interatomic distances and angles are listed in Table 1.

As the overall molecular structures of the heptanuclear complexes in **1** and **2** are closely related, only the molecular structure of $^{RR}[Fe^{III}_6Fe^{II}]^{2+}$ in **2** is shown in Fig. 2. The heptanuclear complexes in **1** and **2** consist of two trinuclear triplesalen complexes bridged by a central hexacyanoferrate. The terminal metal ions, Mn^{III} in **1** and Fe^{III} in **2**, are coordinated by the N_2O_2 salen-like coordination compartment, a nitrogen of the bridging hexacyanoferrate, and an oxygen donor from solvent molecules. In the asymmetric unit of **1**, all three Mn^{III} ions are coordinated by a dioxane molecule, while in the asymmetric unit of **2** Fe1 and Fe2 are coordinated by a dioxane molecule and Fe3 is coordinated by a methanol molecule. However, it should be mentioned that - despite the coordinated methanol with an Fe-O distance of 2.20 Å - the M-O(dioxane) distances are extremely long in the range 2.65 to 2.88 Å. In both crystal structures, the heptanuclear complexes are bridged by one dioxane molecule, which is coordinated to Mn1 in **1** and Fe2 in **2**, leading to one-dimensional chains along the crystallographic *c* axis (Fig. S2). This results in angles between the approximate molecular C_3 axes of the heptanuclear

complexes in **1** and **2** of 45.2° and 52.0°, respectively. These and other selected structural parameters are summarized in Table 2.

In order to gain an understanding of the differences of the molecular structures of heptanuclear complexes obtained with the ligands $(talen^{t\text{-}Bu_2})^{6-}$ and $(chand^{RR})^{6-}$, the molecular structures of $^{RR}[Mn^{III}_6Fe^{II}]^{2+}$ and $^{RR}[Fe^{III}_6Fe^{II}]^{2+}$ are also compared to those of $[Mn^{III}_6Fe^{II}]^{2+}$ and the oxidized complex $[Mn^{III}_6Fe^{III}]^{3+}$,[17b] as an example of the tricationic complexes $[Mn^{III}_6M^{c}]^{3+}$ (Table 2). The Mn^{III}-ligand distances do not differ significantly between $^{RR}[Mn^{III}_6Fe^{II}]^{2+}$ and $[Mn^{III}_6Fe^{II}]^{2+}$, but comparing $^{RR}[Mn^{III}_6Fe^{II}]^{2+}$ to $^{RR}[Fe^{III}_6Fe^{II}]^{2+}$, the distances for Fe-$N^{cent}$ = 2.15 Å and Fe-N^{term} = 2.08 Å are significantly longer than the corresponding values for Mn-N^{cent} = 2.03 Å and Mn-N^{term} = 1.97 Å. This difference in the metal-nitrogen bond distances has already been observed in the mononuclear complexes $[(chand^{RR})\{MnCl\}_3]$ and $[(chand^{RR})\{FeCl\}_3]$. Moreover, the Mn-$N^{C\equiv N}$ bond distances vary significantly, and their mean value (2.13 Å) is significantly higher than that of the Fe-$N^{C\equiv N}$ bond distance (2.02 Å). This can be attributed to the Jahn-Teller distortion of Mn^{III} (tetragonally elongated octahedron) with Mn-$N^{C\equiv N}$ and Mn-$N^{solvent}$ forming the Jahn-Teller axis.

In contrast to this inner-sphere coordination, which exhibits no significant change when going from $(talen^{t\text{-}Bu_2})^{6-}$ to $(chand^{RR})^{6-}$, the overall arrangement of the metal-salen subunits differs strongly. Figure 3 shows different orientations of a representative Mn-salen subunit of $^{RR}[Mn^{III}_6Fe^{II}]^{2+}$ and $[Mn^{III}_6Fe^{II}]^{2+}$ to illustrate the various types of structural distortions. In our previous work, we identified some parameters suitable to obtain a quantitative description of the ligand folding in our triplesalen complexes. The bent angle φ (introduced by Cavallo and Jacobsen for salen complexes)[26] is defined by $\varphi = 180° - \angle(M–X_{NO}–X_R)$ (X_{NO}: midpoint of adjacent N and O donor atoms; X_R: midpoint of the six-membered chelate ring containing the N and O donor atoms) and is best suited to

differentiate between a bending along an idealized line through neighboring N and O ligands and a line perpendicular to the former resulting in a helical distortion. In the heptanuclear complexes **[$Mn^{III}_6Cr^{III}$]$^{3+}$**, **[$Mn^{III}_6Mn^{III}$]$^{3+}$**, **[$Mn^{III}_6Fe^{III}$]$^{3+}$**, and **[$Mn^{III}_6Co^{III}$]$^{3+}$** of (talen$^{t\text{-}Bu_2}$)$^{6-}$, the terminal phenolates exhibit only a small bending (φ^{term} = 8 - 10°), while there is a significantly stronger bending at the central phloroglucinol (φ^{cent} = 36 - 47°). The positive sign for both angles indicates folding to the same side with respect to the $Mn^{III}N_2O_2$ coordination plane, resulting in the overall bowl-shaped molecular structure of the trinuclear triplesalen building blocks (Fig. 3b). The mean bent angles φ^{cent} and φ^{term} are +24.6 and -22.3° for **1** and +28.6 and -21.3° for **2**, respectively. The negative sign of φ^{term} illustrates bending towards the opposite site with φ^{cent} as a reference (Fig. 3a). The different signs of φ^{cent} and φ^{term} for both **1** and **2** are related to the overall 'soup plate-shaped' molecular structure of the trinuclear triplesalen building blocks in these complexes.

A parameter describing the helical distortion of the M^t-salen subunits, is the angle θ, which is defined as the angle between the benzene plane of the central phloroglucinol and the vector formed by the central phenolate O atom and the central ketimine N atom.[18] These angles are much larger for **1** and **2** as compared to the (talen$^{t\text{-}Bu_2}$)$^{6-}$ complexes (Table 2). This different helical distortion is best illustrated in the central panel of Figure 3.

The different distortions of the trinuclear M^t-triplesalen building blocks in 1 and 2 compared to the heptanuclear complexes of the ligand (talen$^{t\text{-}Bu_2}$)$^{6-}$ also impact the structure of the central hexacyanoferrate, which has a stronger trigonal compression in **1** and **2** as evidenced by the larger angle C-Fe-C with the carbon atoms belonging to cyanides bound to the same trinuclear triplesalen subunit (Table 2). Besides this compression, the Fe-C≡N units are less linear in **1** and **2**. However, the strongest

difference is in the angle C≡N-M^t (Table 2), which is best illustrated in the right panel of Figure 3.

The heteroradialene nature of the triplesalen unit in $\mathbf{[M^t_6M^c]^{n+}}$ has a structural signature in the elongation of the mean C-C bond lengths of the central phloroglucinol ring, which deviates from a typical benzene bond length of ~1.39 Å.[9c] Besides this bond length increase, there is an alternation in bond lengths. This observation indicates a decrease in the aromatic character, which can be quantified by the HOMA value (harmonic oscillator model of aromaticity), which takes a value of 1 for the model aromatic system benzene and of 0 for a model non-aromatic system.[27] $\mathbf{[Mn^{III}_6Fe^{III}]^{3+}}$ with a mean $d(\text{C-C})^{\text{cent}}$ = 1.43 Å and $\text{HOMA}^{\text{cent}}$ = 0.65 is a typical example of the tricationic complexes $\mathbf{[M^t_6M^c]^{3+}}$. The stronger C=O double bond character of the heteroradialene unit is also reflected in the short d(C=O) bond distance of 1.31 Å. We have already observed less heteroradialene character in the dicationic complexes $\mathbf{[M^t_6M^c]^{2+}}$ as evident from the respective structural parameters for $\mathbf{[Mn^{II}_6Fe^{II}]^{2+}}$ in Table 2.[17b] The mean $d(\text{C-C})^{\text{cent}}$ bond lengths and the HOMA values for **1** and **2** indicate even less heteroradialene character in the dicationic heptanuclear complexes of $(\text{chand}^{\text{RR}})^{6-}$.

In summary, the triplesalen ligand $(\text{chand}^{\text{RR}})^{6-}$ induces a different and more significant distortion of the M^t-salen subunits compared to the triplesalen ligand $(\text{talen}^{t\text{-Bu}_2})^{6-}$, resulting in an overall 'soup plate-shaped' as compared to the 'bowl-shaped' molecular structure and a stronger helical folding. This significantly different distortion also affects the structure of the central hexacyanometallate. Most important with regard to the magnetic properties are the variations in the structural parameters of the central phloroglucinol unit indicating that the $(\text{chand}^{\text{RR}})^{6-}$ complexes $\mathbf{^{RR}[M^t_6Fe^{II}]^{2+}}$ exhibit less heteroradialene character in comparison to the $(\text{talen}^{t\text{-Bu}_2})$ complexes $\mathbf{[M^t_6M^c]^{n+}}$.

Mössbauer and UV-vis Spectroscopies

The Mössbauer spectrum of **1a** exhibits a single absorption line (Fig. 4a). However, simulations require a small but non-zero quadrupole splitting (Table 3). This small quadrupole splitting further proves the Fe^{II} oxidation state in **1a** (Table 3) despite the use of $[Fe^{III}(CN)_6]^{3-}$ in the synthesis. Complex **2a** exhibits two absorption lines of different intensities (Fig. 4b). Simulations were carried out using two quadrupole doublets. Without using further constraints, the fitting procedure provides two quadrupole doublets whose intensities are in accordance with the ratio Fe^{t}:Fe^{c} = 6:1. The quadrupole doublet for the central Fe^{II} ion has an intensity of 13.6 %, while the six terminal Fe^{III} ions cover an area of 86.4 %. The central Fe^{II} I. s. exhibits no significant variation compared to the Fe^{II} I. s. of **$[Mn^{III}_6Fe^{II}]^{2+}$** (Table 3). The large quadrupole splitting of 1.50 mm s^{-1} of the terminal Fe^{III} h. s. ions of **2a** is even larger than that of the respective trinuclear complex $[(chand^{RR})\{Fe^{III}Cl\}_3]$ of 1.13 mm s^{-1} (δ = 0.44 mm s^{-1}).

The UV-vis spectra of **$^{RR}[Mn^{III}_6Fe^{II}]^{2+}$** and **$^{RR}[Fe^{III}_6Fe^{II}]^{2+}$** are provided in Figure 5. For comparison, the spectra of the heptanuclear complex **$[Mn^{III}_6Fe^{II}]^{2+}$** and the respective spectra of the trinuclear complexes are also shown. The spectrum of **$^{RR}[Mn^{III}_6Fe^{II}]^{2+}$** closely resembles that of **$[Mn^{III}_6Fe^{II}]^{2+}$**, including the 25000-35000 cm^{-1} region where the heteroradialene character of the central phloroglucinol backbone causes two strong absorption features,[9c] i. e. the differences in the heteroradialene contribution indicated by the structural data (*vide supra*) are not detected in solution. The heptanuclear iron complex **$^{RR}[Fe^{III}_6Fe^{II}]^{2+}$** exhibits pronounced differences in the UV-vis spectrum demonstrating that the main absorption features in these heptanuclear complexes originate from the M^{t}-salen subunits. This is also apparent from the trinuclear analogs whose spectra coincide mostly with those of the heptanuclear complexes with half of their intensity. The strong absorption maximum of **$^{RR}[Fe^{III}_6Fe^{II}]^{2+}$** at 18200 cm^{-1} (ε = 38500 M^{-1}

cm^{-1}) corresponds to the characteristic phenolate-to-Fe^{III} h. s. LMCT transition, which appears at 19250 cm^{-1} (ε = 17850 M^{-1} cm^{-1}) in the trinuclear complex $[(chand^{RR})\{Fe^{III}Cl\}_3]$.[22a]

Electrochemistry

The electrochemical properties of **1a** and **2a** were measured in acetonitrile solution by cyclic (CV) and square-wave (SW) voltammetry. Some representative voltammograms are shown in Figure 6. $^{RR}[Mn^{III}_6Fe^{II}]^{2+}$ in **1a** exhibits irreversible reductions at negative potentials and irreversible oxidations above 1 V vs Fc^+/Fc, which are both typical for the heptanuclear complexes of $(talen^{t\text{-}Bu_2})^{6-}$ with terminal Mn^{III} ions.[16b,17b,20b] Additionally, there is a reversible wave at $E_{1/2}$ = 0.21 V vs Fc^+/Fc, which closely resembles a reversible wave in $[Mn^{III}_6Fe^{II}]^{2+}$ at -0.06 V that has been attributed to the reversible Fe^{III}/Fe^{II} redox couple of the central hexacyanoferrate. At negative potentials, $^{RR}[Fe^{III}_6Fe^{II}]^{2+}$ in **2a** exhibits a larger number of irreversible reductions than $^{RR}[Mn^{III}_6Fe^{II}]^{2+}$ whereas it shows almost the same features in the oxidative range above 1 V vs Fc^+/Fc, which corroborates previous findings that these oxidations are ligand-centered.[16,17b,19] Most interestingly, a reversible wave is observed at $E_{1/2}$ = 0.75 V vs Fc^+/Fc.

The free hexacyanoferrates exhibit the redox couple $[Fe^{III}(CN)_6]^{3-}/[Fe^{II}(CN)_6]^{4-}$ in acetonitrile at $E_{1/2}$ = -1.01 V vs Fc^+/Fc. We have commonly observed a shift of approximately +0.9 V for the redox potentials of the $[M^c(CN)_6]^{n-}$ unit as a result of its encapsulation by two tricationic triplesalen building blocks in $[Mn^{III}_6M^c]^{(6-n)+}$ due to the increasing tendency of a redox-active unit to be reduced when the overall positive charge is increased.[16,17b,19,20b] Using the triplesalen ligand $(chand^{RR})^{6-}$ instead of $(talen^{t\text{-}Bu_2})^{6-}$ does not influence the overall charge of the heptanuclear complex. Therefore, the shift of the redox potential of the central hexacyanoferrate unit from -0.06 to +0.21 V vs Fc^+/Fc

when going from $\mathbf{[Mn^{III}_6Fe^{II}]^{2+}}$ to $\mathbf{^{RR}[Mn^{III}_6Fe^{II}]^{2+}}$ indicates a stabilization of the reduced central hexacyanometallate in heptanuclear complexes of the ligand $(chand^{RR})^{6-}$, which reflects the structural changes of the hexacyanometallate induced by the stronger distortions of the trinuclear triplesalen building blocks.

However, the shift of the redox potential of the central hexacyanoferrate to +0.75 V in $\mathbf{^{RR}[Fe^{III}_6Fe^{II}]^{2+}}$ that comes along with the change of the terminal ions from Mn^{III} to Fe^{III} is remarkable. This significant destabilization of the central oxidized Fe^{III} l. s. ion might be attributed to the stronger electron donation of the coordinated cyanides to the terminal Fe^{III} h. s. ion (d(Fe-$N^{N\equiv C}$) = 2.02 Å) in comparison to the terminal Jahn-Teller distorted Mn^{III} (d(Mn-$N^{N\equiv C}$) = 2.13 Å).

Magnetic Properties

Direct current (DC) and alternating current (AC) magnetization measurements have been performed on **1a** and **2a** under various experimental conditions. The DC magnetic properties were simulated by a full-matrix diagonalization of the spin-Hamiltonian given in equation (1).

$$\hat{H} = -2\sum_{i<j} J_{ij}\,\hat{\mathbf{S}}_i \cdot \hat{\mathbf{S}}_j \quad + \quad \sum_i D_i \left(\hat{\mathbf{S}}_i \cdot \mathbf{e}_i(\vartheta_i,\varphi_i)\right)^2 \quad + \quad \mu_B \sum_i \mathbf{B} \cdot \underline{\underline{\mathbf{g}}}_i \cdot \hat{\mathbf{S}}_i \qquad (1)$$

The first term reflects the isotropic exchange interaction between spins given by the spin vector operators $\hat{\mathbf{S}}_i$ at sites i. Complexes $\mathbf{^{RR}[Mn^{III}_6Fe^{II}]^{2+}}$ in **1a** and $\mathbf{^{RR}[Fe^{III}_6Fe^{II}]^{2+}}$ in **2a** consist of six terminal spins $S_i \neq 0$, while the central metal ion is diamagnetic. We have already analyzed this spin structure in $\mathbf{[Mn^{III}_6Co^{III}]^{3+}}$ [18] and $\mathbf{[Mn^{III}_6Fe^{II}]^{2+}}$.[17b] Our studies showed that not only the coupling between the paramagnetic ions within one triplesalen subunit (intra-triplesalen coupling) needs to be considered but also the coupling between the paramagnetic ions within two different triplesalen subunits (inter-triplesalen coupling).

By symmetry, two different inter-triplesalen couplings must be considered, which are visualized by the coupling scheme provided in Scheme 3.

The second term in equation (1) reflects the local zero-field splitting tensors. These tensors are parameterized by a strength factor D_i as well as by unit vectors $\mathbf{e}_i$, which are parameterized by polar angles ϑ_i and φ_i. The unit vectors of the six Mn^{III} ions point along their local Jahn-Teller axis. Because of the approximate S_6 symmetry, all six local unit vectors $\mathbf{e}_i$ can be parameterized by the common polar angle ϑ between the Jahn-Teller axis and the S_6 symmetry axis, which has been extracted from the crystal structures and is provided in Table 2.

The third term of equation (1) represents the Zeeman term. Isotropic g values of g = 1.98 and g = 1.99 have been used for the Mn^{III} ions of $^{RR}[Mn^{III}_6Fe^{II}]^{2+}$ and the Fe^{III} ions of $^{RR}[Fe^{III}_6Fe^{II}]^{2+}$, respectively. In the presence of a magnetic field, we employ inversion symmetry. Powder average has been taken into account by an orientational average based on isotropic or Lebedev-Laikov grids with up to 50 orientations.[28]

$^{RR}[Mn^{III}_6Fe^{II}]^{2+}$. The effective magnetic moment, μ_B, of **1a** is 11.89 μ_B at 287 K (Fig. 7a), which almost coincides with the theoretical value of 11.88 μ_B for six uncoupled Mn^{III} ions (S_i = 2, g_i = 1.98). By decreasing the temperature, μ_{eff} increases very slightly until 80 K and then exhibits a stronger increase to a maximum of 12.64 μ_B at 5 K. Further temperature decrease results in a decrease of μ_{eff} to 10.86 μ_B at 2.1 K. This temperature-dependence indicates ferromagnetic interactions between the Mn^{III} ions. It should be noted that the analog complex of $(talen^{t\text{-}Bu_2})^{6-}$ **$[Mn^{III}_6Fe^{II}]^{2+}$** exhibits antiferromagnetic interactions between the Mn^{III} ions.[17b] We have simulated the temperature-dependence of μ_{eff} in conjunction with the variable temperature-variable field (VTVH) measurements, which exhibit a slight nesting behavior (Fig. 7b). The first simulations were performed using only J_1 (intra-triplesalen coupling) and D_{Mn} yielding a qualitative reproduction of the

experimental data. However, in analogy to **[Mn$^{III}_6$Co^{III}]$^{3+}$** [18] and **[Mn$^{III}_6$Fe^{II}]$^{2+}$**,[17b] the simulations incorporating J_2 and J_3 provide a better reproduction of the experimental data. We thus performed several simulations varying J_1, J_2, J_3, and D_{Mn}. It turned out that not only J_1 is ferromagnetic, but also the sum of J_2 and J_3 is slightly ferromagnetic. Unfortunately, the exact distribution of J_2 and J_3 is not determined by the experimental data. A small set of our simulations is provided in Figure 7, demonstrating the influence of J_2, J_3, and D_{Mn}. The careful evaluation of all simulations provides a good understanding of the influence of each parameter on the simulated curves and allows an estimation of the parameters including an error range: J_1 = +0.17±0.02 cm^{-1} and D_{Mn} = -3.4±0.3 cm^{-1}. J_2 and J_3 are correlated such that their sum is smaller than 0.04 cm^{-1}.

Interestingly, **1a** exhibits the onset of a frequency-dependence of χ'' at temperatures below 2.3 K indicating a slow relaxation of the magnetization, which is a typical property of a single-molecule magnet (Fig. 8). It should be noted that we do not seek to emphasize that **^{RR}[Mn$^{III}_6$Fe^{II}]$^{2+}$** is a single-molecule magnet but rather that the relatively small change in the intra-triplesalen Mn^{III}-Mn^{III} coupling from J_1 = -0.20 to +0.17 cm^{-1} when going from **[Mn$^{III}_6$Fe^{II}]$^{2+}$** to **^{RR}[Mn$^{III}_6$Fe^{II}]$^{2+}$** is sufficient to provide an energy barrier for spin reversal that can be detected by AC susceptibility measurements.

^{RR}[Fe$^{III}_6$Fe^{II}]$^{2+}$. Compound **2a** exhibits μ_{eff} = 14.47 μ_B at 287 K corresponding well with the value of 14.42 μ_B calculated for six uncoupled Fe^{III} h. s. ions (S_i = 5/2, g_i = 1.99). By decreasing the temperature, μ_{eff} increases slightly until 80 K and then increases more rapidly to a value of 18.89 μ_B at 5 K (Fig. 9a). This temperature-dependence is again typical for ferromagnetic interactions. In analogy to **^{RR}[Mn$^{III}_6$Fe^{II}]$^{2+}$** we simulated the temperature-dependence of μ_{eff} and the VTVH data with spin-Hamiltonian equation (1) varying J_1, J_2, J_3, and D_{Fe}. As expected for Fe^{III} h. s., no zero-field splitting D_{Fe} appeared necessary. Some of our simulations are provided in Figure 9. In an analogous procedure

to ^{RR}**[Mn$^{III}_6$Fe^{II}]$^{2+}$** the following values have been extracted from the simulations for ^{RR}**[Fe$^{III}_6$Fe^{II}]$^{2+}$**: J_1 = +0.235±0.005 cm^{-1}, J_2 = -0.03±0.01 cm^{-1}, J_3 = +0.04±0.01 cm^{-1}, and D_{Fe} = 0.

For the trinuclear Fe^{III} complexes of (talen$^{t\text{-}Bu_2}$)$^{6-}$ [22b] and (chand^{RR})$^{6-}$,[22a] the magnetic measurements indicated almost no coupling between the ferric ions. Therefore, it is interesting to note that for ^{RR}**[Mn$^{III}_6$Fe^{II}]$^{2+}$**, which represents the first heptanuclear triplesalen complex with terminal Fe^{III} h. s. ions, a ferromagnetic coupling is observed.

Conclusions

The trinuclear complexes [(chand^{RR})M^t(solv)$_n$]$^{3+}$ (M^t = Mn^{III}, Fe^{III}) of the chiral triplesalen ligand (chand^{RR})$^{6-}$ can be bridged by a central hexacyanoferrate to yield the heptanuclear complexes ^{RR}**[Mn$^{III}_6$Fe^{II}]$^{2+}$** and ^{RR}**[Fe$^{III}_6$Fe^{II}]$^{2+}$**. Although the synthetic protocol employs ferric [Fe^{III}(CN)$_6$]$^{3-}$, encapsulation in the heptanuclear complexes results in the reduction to a bridging ferrous [Fe^{II}(CN)$_6$]$^{4-}$. The strong stabilization of the reduced form is reflected in the results from electrochemical measurements, which exhibit shifts of the redox potential relative to the free [Fe$^{III/II}$(CN)$_6$]$^{3-/4-}$ redox couple of +1.22 and +1.76 V as a consequence of the encapsulation of the hexacyanoferrate in ^{RR}**[Mn$^{III}_6$Fe^{II}]$^{2+}$** and ^{RR}**[Fe$^{III}_6$Fe^{II}]$^{2+}$**, respectively. The straightforward formation of the heptanuclear complexes ^{RR}**[Mn$^{III}_6$Fe^{II}]$^{2+}$** and ^{RR}**[Fe$^{III}_6$Fe^{II}]$^{2+}$** was unexpected as the heptanuclear complexes of the achiral triplesalen ligand (talen$^{t\text{-}Bu_2}$)$^{6-}$ **[M$^t_6$M^c]$^{n+}$** are of S_6 symmetry with a center of inversion at the central hexacyanometallate. However, the heptanuclear complexes ^{RR}**[Mn$^{III}_6$M^c]$^{2+}$** form from two [(chand^{RR})Mn$^{III}_3$]$^{3+}$ building blocks along with a symmetry reduction from S_6 to C_2 with the C_2 axis being perpendicular to the approximate molecular C_3 axis.

Although the inner-sphere coordination does not change significantly upon going from the achiral ligand (talen$^{t\text{-Bu}_2}$)$^{6-}$ to the chiral ligand (chand^{RR})$^{6-}$, the second coordination sphere of the M^t-salen subunits differs strongly. While the two phenolate rings in the (talen$^{t\text{-Bu}_2}$)$^{6-}$ complexes are bent to the same side of the central M^{t}N$_2$O$_2$ plane resulting in bowl-shaped structures of the trinuclear subunits, the two phenolate rings in the (chand^{RR})$^{6-}$ complexes are bent to opposite sides of the central M^{t}N$_2$O$_2$ plane, which leads to "soup plate-shaped" molecular structures of the trinuclear building blocks. Besides this different ligand folding, there is a stronger helical distortion in the M^t-salen subunits of the (chand^{RR})$^{6-}$ complexes. These significant differences in the structure of the trinuclear triplesalen building blocks also affect the structural details of the central hexacyanoferrate. On the one hand, the central hexacyanoferrate octahedron is more compressed along the approximate molecular C_3 axis in the (chand^{RR})$^{6-}$ complexes; on the other hand, the Fe-C≡N-M^t unit deviates more from linearity with smaller Fe-C≡N and C≡N-M^t angles. These distortions are also reflected in the infrared spectra by values of 2041 vs 2076 cm^{-1} for the ν(C≡N) modes in ^{RR}**[Mn$^{III}_6$Fe^{II}]$^{2+}$** and **[Mn$^{III}_6$Fe^{II}]$^{2+}$**, respectively. A significant difference between ^{RR}**[Mn$^{III}_6$Fe^{II}]$^{2+}$** and ^{RR}**[Fe$^{III}_6$Fe^{II}]$^{2+}$** is in the M^t-N$^{N\equiv C}$ bond distance, which is much longer (2.13 Å) in ^{RR}**[Mn$^{III}_6$Fe^{II}]$^{2+}$** due to the Mn^{III} Jahn-Teller axis in this direction, while it is much shorter (2.02 Å) in ^{RR}**[Fe$^{III}_6$Fe^{II}]$^{2+}$**.

Interestingly, these differences in the molecular structures are also reflected in the redox potential of the central hexacyanoferrate unit, which shifts from -0.06 V in **[Mn$^{III}_6$Fe^{II}]$^{2+}$** to +0.21 V in ^{RR}**[Mn$^{III}_6$Fe^{II}]$^{2+}$** indicating further stabilization of the reduced species. This effect is even more pronounced in ^{RR}**[Fe$^{III}_6$Fe^{II}]$^{2+}$** ($E_{1/2}$ = +0.75 V), which can be attributed to the stronger electron donation of the coordinated cyanides to the terminal Fe^{III} h. s. ions due to the shorter Fe-N$^{N\equiv C}$ bond distances compared to d(Mn-N$^{N\equiv C}$) in ^{RR}**[Mn$^{III}_6$Fe^{II}]$^{2+}$**.

Interestingly, the complexes of the chiral ligand $(chand^{RR})^{6-}$ exhibit less heteroradialene character than their achiral counterparts. This is evidenced by a decrease of the C-C bond lengths of the central phloroglucinol unit in conjunction with an increase of the HOMA value.

Most significant, however, is the strong impact of the weaker heteroradialene contribution in $^{RR}[Mn^{III}_6Fe^{II}]^{2+}$ and $^{RR}[Fe^{III}_6Fe^{II}]^{2+}$ on the magnetic properties of these compounds as it induces a switching from the antiferromagnetic intra-triplesalen coupling observed for the $(talen^{t\text{-}Bu_2})^{6-}$ compounds to a ferromagnetic coupling in the $(chand^{RR})^{6-}$ compounds. The weaker heteroradialene character and therefore increased aromatic character of the central phloroglucinol backbone should give rise to a more efficient spin-polarization contribution to the overall coupling between the M^t ions in a trinuclear building block. Comparing all our available heptanuclear complexes with six terminal Mn^{III} ions and a central Fe ion, there seems to be almost a magnetostructural correlation: upon going from $[Mn^{III}_6Fe^{III}]^{3+}$ to $[Mn^{III}_6Fe^{II}]^{2+}$ and further to $^{RR}[Mn^{III}_6Fe^{II}]^{2+}$, the HOMA value increases from 0.65 to 0.79 and to 0.85, which correlates with a change in $J_{Mn\text{-}Mn}$ from -1.00 cm^{-1} to -0.20 cm^{-1} and to +0.17 cm^{-1}. Importantly, the very small absolute change in $J_{Mn\text{-}Mn}$ when going from $[Mn^{III}_6Fe^{II}]^{2+}$ to $^{RR}[Mn^{III}_6Fe^{II}]^{2+}$ is sufficient to provide a magnetic anisotropy barrier for slow magnetic relaxation indicative of single-molecule magnet behavior of $^{RR}[Mn^{III}_6Fe^{II}]^{2+}$.

As we have realized that the spin-polarization mechanism is not efficient in our triplesalen-based complexes due to heteroradialene formation,[9c] we have started two independent projects involving elaborate organic syntheses to suppress this heteroradialene formation.[29] These projects are synthetically very demanding, but we are convinced that they are worthwhile as we could demonstrate that even a small reduction

of the heteroradialene contribution is sufficient to switch the exchange coupling from antiferromagnetic to ferromagnetic.

Acknowledgements

This work was supported by the DFG (FOR945 “Nanomagnets”), the Fonds der Chemischen Industrie, and Bielefeld University. Veronika Hoeke also gratefully acknowledges the Fonds der Chemischen Industrie for a doctoral fellowship.

Table of contents entry

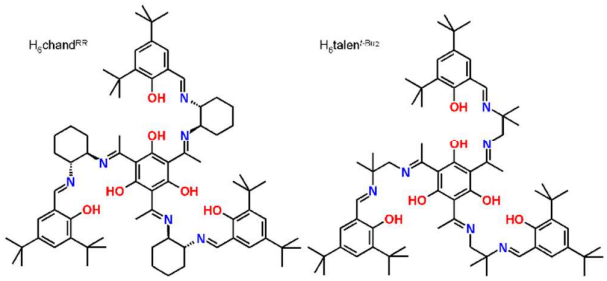

The heptanuclear complexes $[(chand^{RR})_2M^t_6\{Fe^{II}(CN)_6\}]^{2+}$ (M^t = Mn^{III}, Fe^{III}) exhibit ferromagnetic interactions due to a more efficient spin-polarization mechanism compared to the complexes $[(talen^{t\text{-}Bu_2})_2M^t_6\{M^c(CN)_6\}]^{n+}$ with antiferromagnetic interactions.

Table 1. Selected interatomic distances [Å] and angles [°] in **1** and **2**.

	1, M = Mn	**2**, M = Fe
M1-O11	1.875(3)	1.889(3)
M1-O12	1.883(3)	1.893(4)
M2-O21	1.877(2)	1.887(3)
M2-O22	1.900(2)	1.890(3)
M3-O31	1.879(2)	1.897(3)
M3-O32	1.879(3)	1.908(3)
M1-N11	2.030(3)	2.137(4)
M1-N12	1.969(3)	2.075(4)
M2-N21	1.877(2)	2.142(3)
M2-N22	1.970(3)	2.076(4)
M3-N31	2.027(3)	2.160(4)
M3-N32	1.960(3)	2.091(4)
M1-N41	2.116(3)	2.003(4)
M2-N42	2.154(3)	1.990(3)
M3-N43	2.117(3)	2.059(3)
Fe1/Fe4-C41[a]	1.909(4)	1.904(4)
Fe1/Fe4-C42[a]	1.933(4)	1.887(4)
Fe1/Fe4-C43[a]	1.910(4)	1.918(4)
C41-N41	1.173(4)	1.151(6)
C42-N42	1.146(4)	1.177(5)
C43-N43	1.153(5)	1.158(5)
C1-C2	1.419(5)	1.397(7)
C2-C3	1.406(5)	1.420(7)
C3-C4	1.408(6)	1.388(6)
C4-C5	1.418(5)	1.415(6)
C5-C6	1.409(5)	1.414(6)
C1-C6	1.411(6)	1.416(6)
C1-O11	1.334(4)	1.327(6)
C101-O12	1.320(5)	1.309(6)
C3-O21	1.324(5)	1.336(5)
C201-O22	1.321(4)	1.323(6)
C5-O31	1.326(5)	1.333(5)
C301-O32	1.306(5)	1.305(5)
C2-C11	1.454(6)	1.485(6)
C4-C21	1.482(5)	1.478(6)
C6-C31	1.481(5)	1.477(7)
C19-C102	1.445(5)	1.416(9)
C29-C202	1.431(5)	1.446(6)
C39-C302	1.429(6)	1.457(7)
C11-N11	1.306(5)	1.301(6)
C21-N21	1.288(5)	1.298(6)
C31-N31	1.306(5)	1.305(6)
C19-N12	1.288(5)	1.261(7)
C29-N22	1.297(5)	1.276(6)
C39-N32	1.281(5)	1.291(6)
M1•••M2	6.5691(3)	6.5069(4)
M1•••M3	6.6137(2)	6.4757(3)
M2•••M3	6.5614(2)	6.5439(4)

M1•••Fe1/Fe4[a]	4.932(1)	4.868(1)
M2•••Fe1/Fe4[a]	4.983(1)	4.844(1)
M3•••Fe1/Fe4[a]	4.935(1)	4.964(1)
N12-M1-O11	161.75(12)	153.53(15)
N11-M1-O12	159.13(11)	153.49(15)
N22-M2-O21	164.66(13)	154.29(14)
N21-M2-O22	164.89(11)	154.84(13)
N32-M3-O31	162.50(12)	162.88(14)
N31-M3-O32	162.17(12)	162.73(13)
Fe1-C41-N41	172.8(3)	
Fe1-C42-N42	173.4(3)	
Fe1-C43-N43	174.6(3)	
Fe4-C41-N41		175.2(4)
Fe4-C42-N42		174.2(4)
Fe4-C43-N43		174.9(3)
M1-N41-C41	142.0(3)	147.5(4)
M2-N42-C42	143.7(3)	144.9(3)
M3-N44-C43	144.1(3)	150.3(3)

[a] Fe1 for **1**, Fe4 for **2**.

Table 2. Selected structural parameters of compounds.

compound	**1**	**2**	$[Mn^{III}_6Fe^{II}]^{2+}$ [c]	$[Mn^{III}_6Fe^{III}]^{3+}$ [d]
$\angle(C_3^{(1)},C_3^{(2)})$ / ° [a]	45.2	52.0	4.5/70.4/70.6	69.1
shortest intermolecular $M^c\cdots M^c$ distance / Å	16.83	17.07	18.72	18.35
shortest intermolecular $M^t\cdots M^t$ distance / Å	7.89	8.00	10.86	8.63
coordination number of M^t	6	6	5 or 6	6
$d(M^t{-}N^{C\equiv N})$ / Å [b]	2.13	2.02	2.09	2.21
d(Fe−C) / Å [b]	1.92	1.90	1.89	1.94
d(C≡N) / Å [b]	1.16	1.16	1.16	1.15
∠(Fe−C≡N) / ° [b]	173.6	174.8	178.0	179.2
$\angle(C{\equiv}N{-}M^t)$ / ° [b]	143.3	147.6	159.3	162.2
∠(C−Fe−C) / ° [b]	93.1	92.9	90.0	91.2
φ^{cent} / ° [b]	24.6	28.6	41.5	37.3
φ^{term} / ° [b]	-22.3	-21.3	14.8	8.8
θ / ° [b]	27.0	24.9	14.8	8.8
ϑ / ° [b]	41.8	40.9	40.6	38.4
$d(C\text{-}C)^{cent}$ [b]	1.41	1.40	1.42	1.43
$HOMA^{cent}$	0.85	0.86	0.79	0.65
$d(C\text{-}O^{cent})$ / Å [b]	1.33	1.33	1.33	1.31
$d(M^t\text{-}O^{cent})$ / Å [b]	1.88	1.89	1.89	1.89
$d(M^t\text{-}O^{term})$ / Å [b]	1.89	1.90	1.90	1.88
$d(M^t\text{-}N^{cent})$ / Å [b]	2.03	2.15	2.00	1.98
$d(M^t\text{-}N^{term})$ / Å [b]	1.97	2.08	1.99	1.98
$d(M^t\text{-}O^{6th})$ / Å [b]	2.80	2.60	2.44	2.37

[a] Angle between the (approximate) molecular C_3 axes of the $[M^t_6Fe^{II}]^{2+}$ complexes in the crystal.
[b] Mean values.
[c] Heptanuclear complexes in crystals of $[\{(talen^{t\text{-}Bu_2})Mn^{III}\}_3\{Fe^{II}(CN)_6\}(MeOH)_4](BPh_4)_2\bullet 3MeOH\bullet$toluene.[17b]
[d] Heptanuclear complexes in crystals of $[\{(talen^{t\text{-}Bu_2})Mn^{III}\}_3\{Fe^{III}(CN)_6\}(MeOH)_6](PF_6)_2(OAc)\bullet 11MeOH$.[17b]

Table 3. Spectroscopic, magnetic, and electrochemical properties of compounds.

compound	**1a**	**2a**	$[Mn^{III}_6Fe^{II}]^{2+}$ [a]	$[Mn^{III}_6Fe^{III}]^{3+}$ [b]
$\delta(Fe^c)$ / mm s^{-1}	-0.03	-0.05	-0.09	-0.06
$\lvert\Delta E_Q(Fe^c)\rvert$ / mm s^{-1}	0.14	0.17	0.12	0.90
$\delta(Fe^t)$ / mm s^{-1}		0.47		
$\lvert\Delta E_Q(Fe^t)\rvert$ / mm s^{-1}		1.50		
$E_{1/2}$ / V *vs* Fc^+/Fc	+0.21	+0.75	-0.06	-0.06
$J_{Mt\text{-}Mt}$ / mm s^{-1}	+0.17 ± 0.02	+0.235 ± 0.005	-0.20 ± 0.05	-1.00 ± 0.15

[a] Ref. [17b]

[b] Ref. [17b]

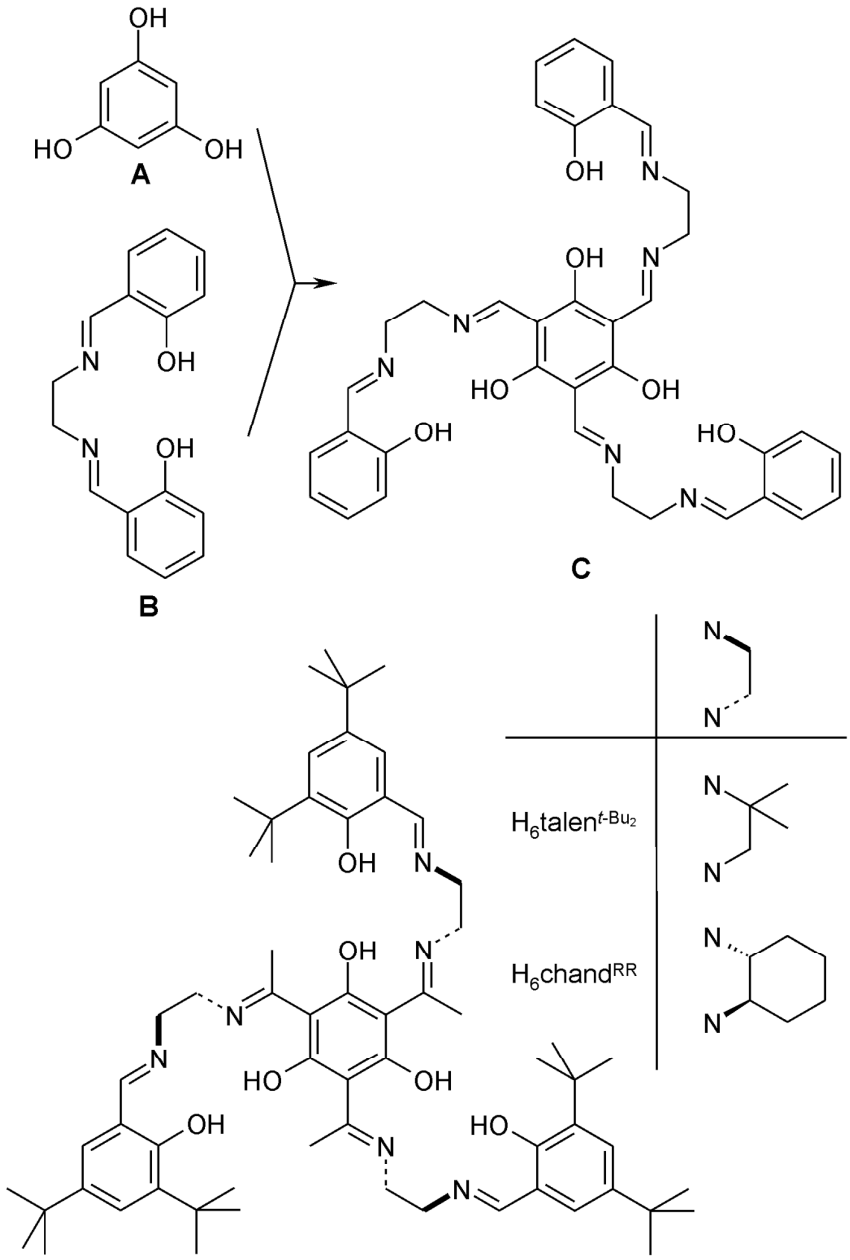

Scheme 1.

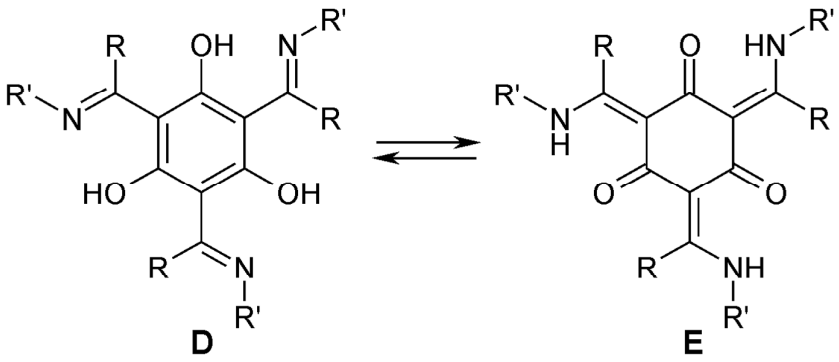

Scheme 2.

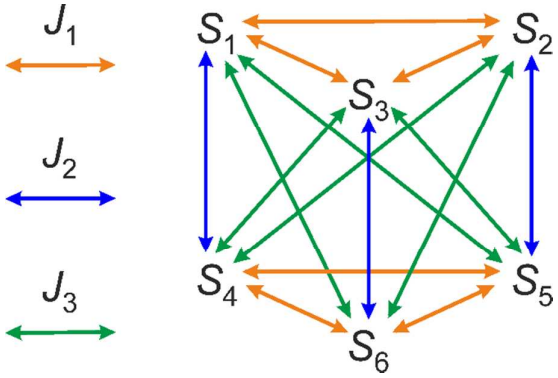

Scheme 3.

Figure 1. Asymmetric units of complexes a) **1** and b) **2**. Non-coordinated solvents, anions, and hydrogen atoms are omitted for clarity.

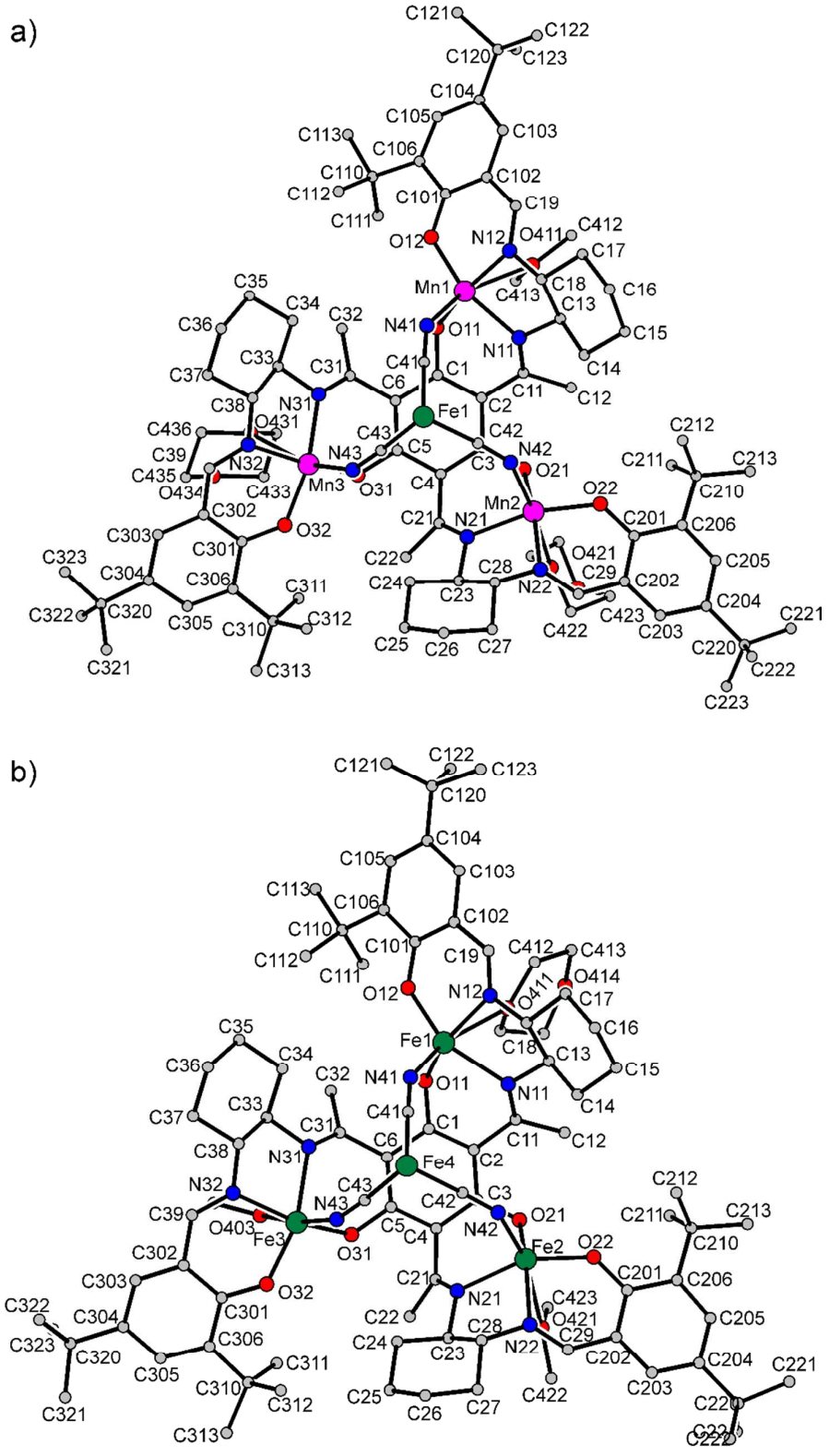

Figure 2. Molecular structure of the heptanuclear complex $[Fe^{III}_6Fe^{II}]^{2+}$ in crystals of **2**. Only the coordinating oxygen atoms of the solvent molecules at the sixth positions of the terminal Fe^{III} ions are shown.

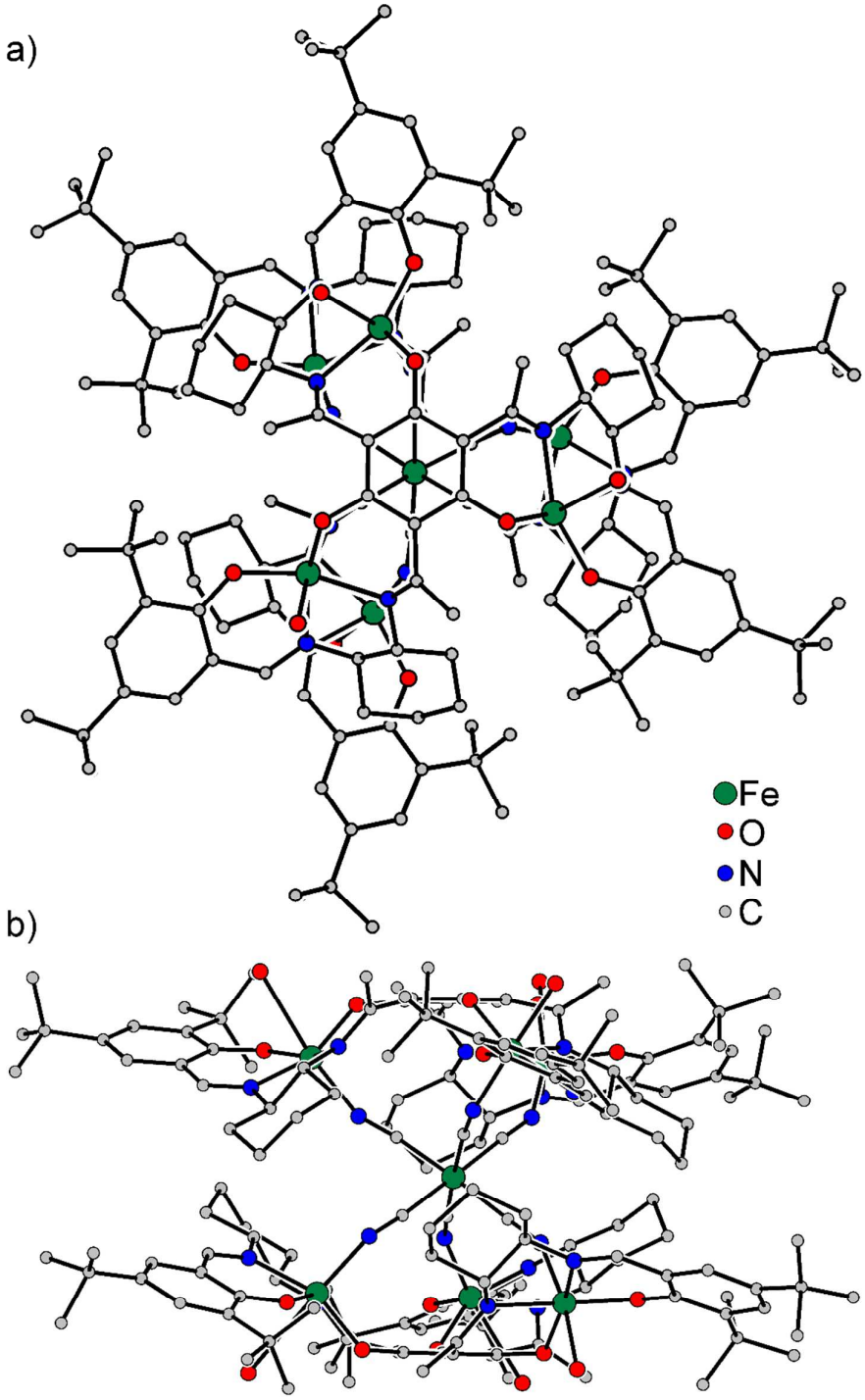

Figure 3. Representative Mn^{III}-salen subunits of a) ^{RR}**[$Mn^{III}_6Fe^{II}$]$^{2+}$** and b) **[$Mn^{III}_6Fe^{II}$]$^{2+}$** to illustrate the different distortions induced by $(chand^{RR})^{6-}$ and $(talen^{t\text{-}Bu_2})^{6-}$, respectively. Left panel: view perpendicular to the central phloroglucinol unit to illustrate the different folding of the terminal phenolates; central panel: related to the left panel but rotated along the molecular C_3 axis; right panel: view perpendicular to the best plane of the salen-like N_2O_2 inner-sphere coordination.

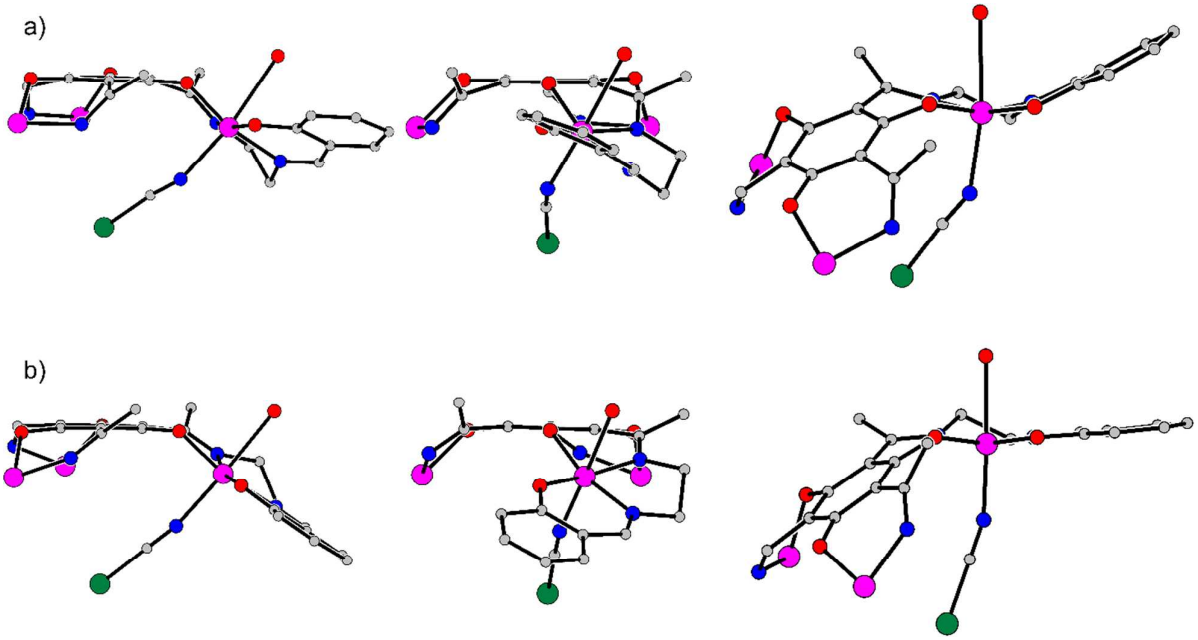

Figure 4. ^{57}Fe Mössbauer spectra of a) **1a** and b) **2a** at 80 K. The solid lines correspond to simulations with the parameters provided in Table 3.

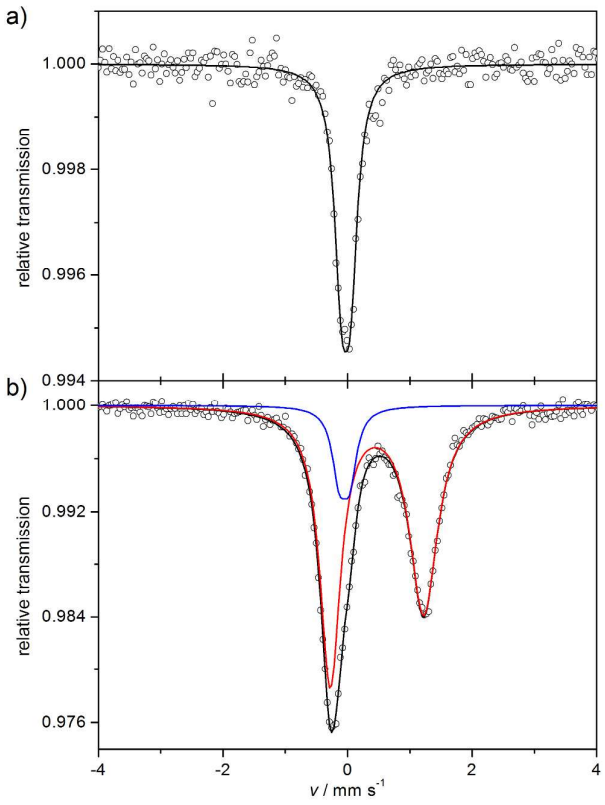

Figure 5. Electronic absorption spectra in acetonitrile solution. The spectrum of [(talen$^{t\text{-}Bu_2}$)Mn^{III}_3(solv)$_n$]$^{3+}$ has been generated *in situ* in acetonitrile.[15]

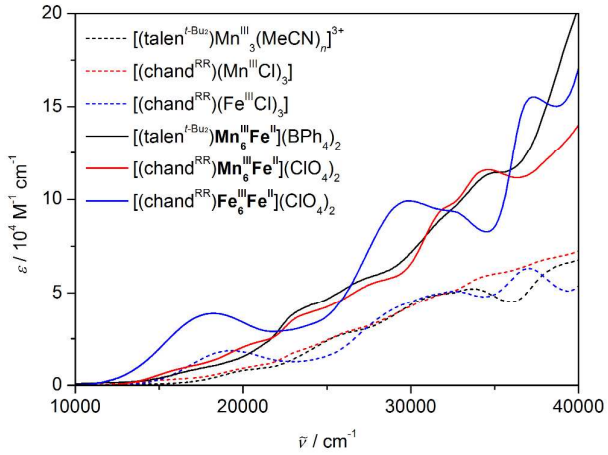

Figure 6. Cyclic voltammograms of a) **1a** and b) **2a** in acetonitrile solution ($(NBu_4)PF_6$, 0.1 M) at 20 °C recorded at a glassy carbon working electrode.

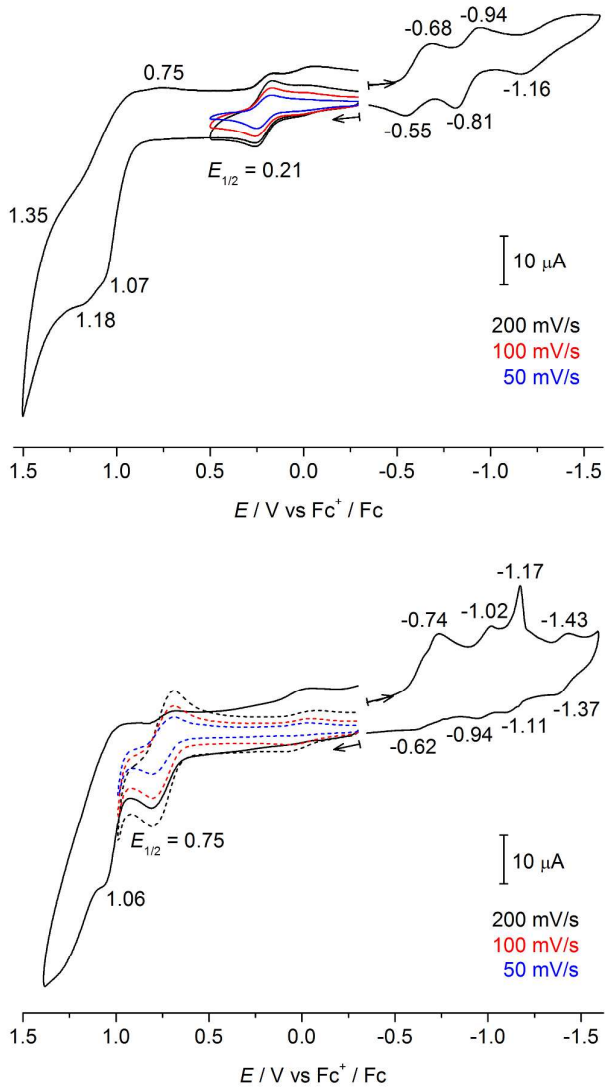

Figure 7. a) Temperature-dependence of μ_{eff} at 1 T, and b) VTVH magnetization measurements at 1, 4, 7 T for **1a**. Experimental data are given as circles. The lines correspond to simulations performed by a full-matrix diagonalization of the spin-Hamiltonian in equation (1) with use of the coupling scheme in Scheme 3. The legend in a) also applies to b). Note that the simulations illustrate the variation of J_2, J_3, and D_{Mn}.

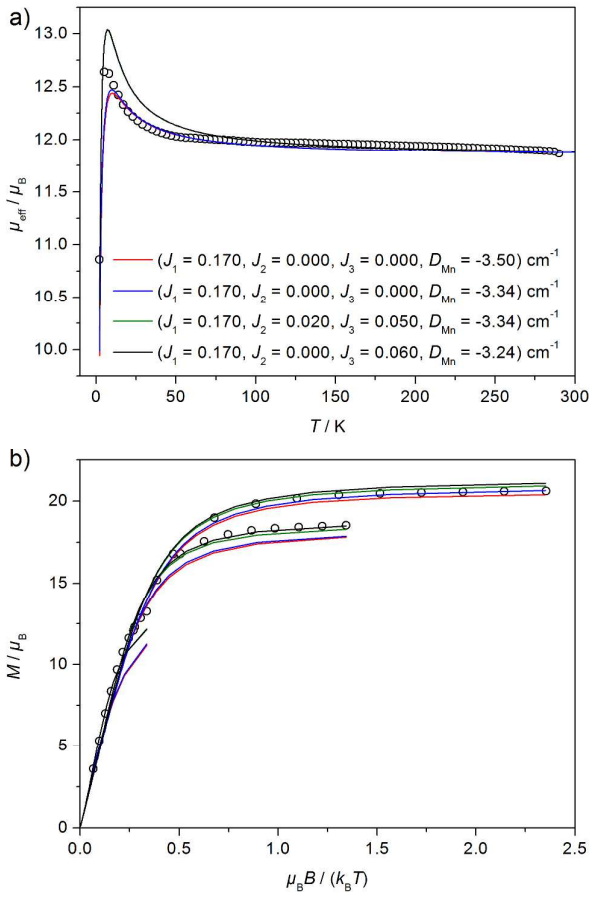

Figure 8. Plots of the in-phase (χ'_M) and the out-of-phase (χ''_M) components of the AC susceptibility vs the temperature for **1a** in zero-DC field with an oscillating AC field of 3 Oe. Solid lines are a guide to the eyes.

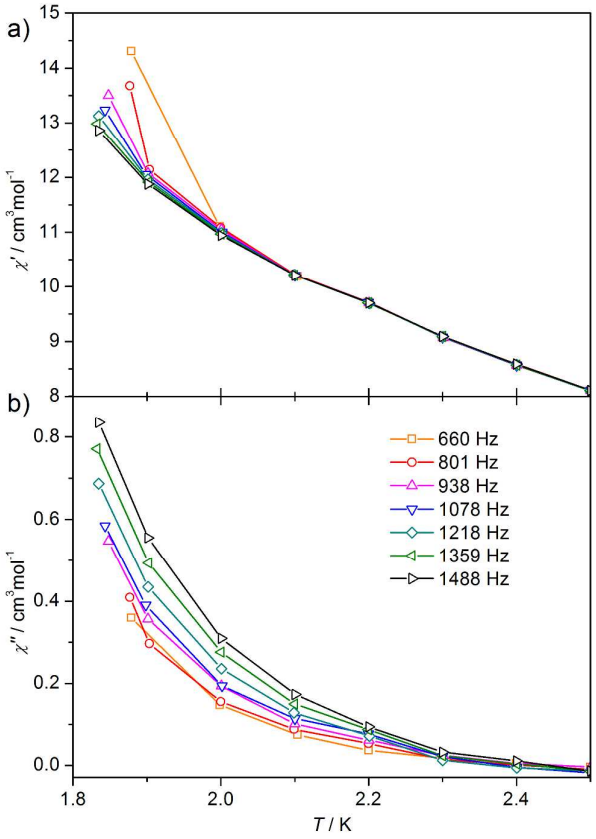

Figure 9. a) Temperature-dependence of μ_{eff} at 1 T, and b) VTVH magnetization measurements at 1,4,7 T, for **2a**. Experimental data are given as symbols. The lines correspond to simulations performed by a full-matrix diagonalization of the spin-Hamiltonian in equation (1) with use of the coupling scheme shown in Scheme 3. Note that the simulations illustrate the influence of J_3.

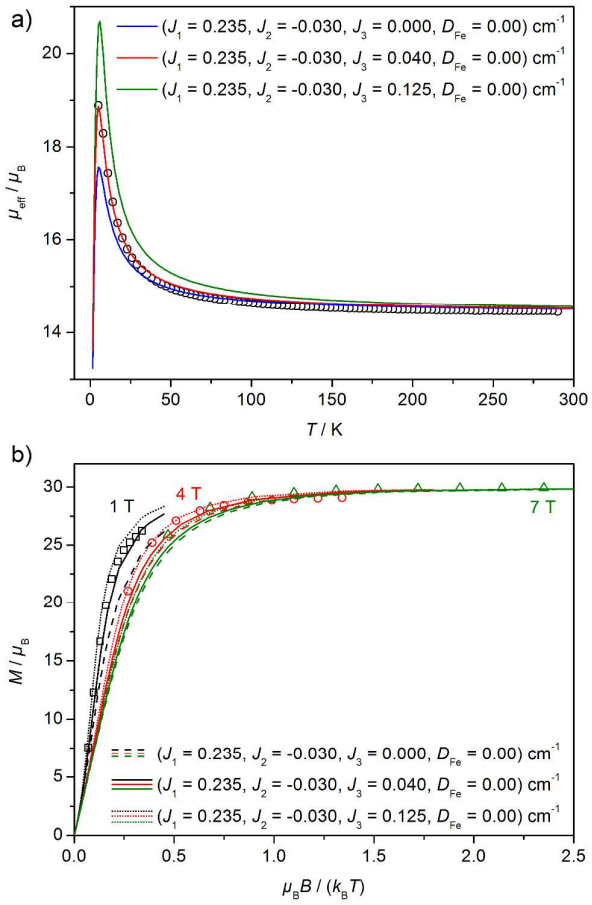

References

1 R. Sessoli, H. L. Tsai, A. R. Schake, S. Y. Wang, J. B. Vincent, K. Folting, D. Gatteschi, G. Christou, D. N. Hendrickson, *J. Am. Chem. Soc.* **1993**, *115*, 1804–1816.

2 a) R. Sessoli, D. Gatteschi, A. Caneschi, M. A. Novak, *Nature* **1993**, *365*, 141–143; b) M. R. Cheesman, V. S. Oganesyan, R. Sessoli, D. Gatteschi, A. J. Thomson, *Chem. Comm.* **1997**, 1677–1678; c) Z. M. Sun, D. Ruiz, E. Rumberger, C. D. Incarvito, K. Folting, A. L. Rheingold, G. Christou, D. N. Hendrickson, *Inorg. Chem.* **1998**, *37*, 4758–4759; d) Z. M. Sun, D. Ruiz, N. R. Dilley, M. Soler, J. Ribas, K. Folting, M. B. Maple, G. Christou, D. N. Hendrickson, *Chem. Comm.* **1999**, 1973–1974; e) McInnes, Eric J. L., E. Pidcock, V. S. Oganesyan, M. R. Cheesman, A. K. Powell, A. J. Thomson, *J. Am. Chem. Soc.* **2002**, *124*, 9219–9228.

3 a) L. Thomas, F. Lionti, R. Ballou, D. Gatteschi, R. Sessoli, B. Barbara, *Nature* **1996**, *383*, 145–147; b) W. Wernsdorfer, R. Sessoli, *Science* **1999**, *284*, 133–135; c) D. Gatteschi, R. Sessoli, *Angew. Chem. Int. Ed.* **2003**, *42*, 268–297; d) A.-L. Barra, A. Caneschi, A. Cornia, D. Gatteschi, L. Gorini, L.-P. Heiniger, R. Sessoli, L. Sorace, *J. Am. Chem. Soc.* **2007**, *129*, 10754–10762; e) D. Gatteschi, R. Sessoli, J. Villain, *Molecular Nanomagnets*, Oxford University Press, Oxford, **2006**; f) W. Wernsdorfer, *Adv. Chem. Phys.* **2001**, *118*, 99–190.

4 a) G. Aromi, E. K. Brechin, *Struct. Bonding* **2006**, *122*, 1–67; b) O. Roubeau, R. Clérac, *Eur. J. Inorg. Chem.* **2008**, 4325–4342; c) J.-N. Rebilly, T. Mallah, *Struct. Bonding* **2006**, *122*, 103–131; d) C. J. Milios, A. Vinslava, W. Wernsdorfer, S. Moggach, S. Parsons, S. P. Perlepes, G. Christou, E. K. Brechin, *J. Am. Chem. Soc.* **2007**, *129*, 2754–2755; e) N. Ishikawa, M. Sugita, T. Ishikawa, S. Koshihara, Y.

Kaizu, *J. Am. Chem. Soc.* **2003**, *125*, 8694–8695; f) J. D. Rinehart, M. Fang, W. J. Evans, J. R. Long, *Nature Chem.* **2011**, *3*, 538–542; g) J. D. Rinehart, M. Fang, W. J. Evans, J. R. Long, *J. Am. Chem. Soc.* **2011**, *133*, 14236–14239.

5 a) H. Heersche, Z. de Groot, J. Folk, van der Zant, H., C. Romeike, M. Wegewijs, L. Zobbi, D. Barreca, E. Tondello, A. Cornia, *Phys. Rev. Lett.* **2006**, *96*; b) M. Mannini, F. Pineider, C. Danieli, F. Totti, L. Sorace, P. Sainctavit, M. A. Arrio, E. Otero, L. Joly, J. C. Cezar, A. Cornia, R. Sessoli, *Nature* **2010**, *468*, 417–421; c) D. Gatteschi, A. Cornia, M. Mannini, R. Sessoli, *Inorg. Chem.* **2009**, *48*, 3408; d) M. Mannini, F. Pineider, P. Sainctavit, C. Danieli, E. Otero, C. Sciancalepore, A. M. Talarico, M. A. Arrio, A. Cornia, D. Gatteschi, R. Sessoli, *Nat. Mater.* **2009**, *8*, 194–197; e) F. Pineider, M. Mannini, C. Danieli, L. Armelao, F. M. Piras, A. Magnani, A. Cornia, R. Sessoli, *J. Mater. Chem.* **2010**, *20*, 187–194; f) R. Vincent, S. Klyatskaya, M. Ruben, W. Wernsdorfer, F. Balestro, *Nature* **2012**, *488*, 357–360; g) L. Bogani, W. Wernsdorfer, *Nat. Mater.* **2008**, *7*, 179–186; h) M. Mannini, P. Sainctavit, R. Sessoli, Cartier dit Moulin, Christophe, F. Pineider, M.-A. Arrio, A. Cornia, D. Gatteschi, *Chem. Eur. J.* **2008**, *14*, 7530–7535.

6 J. Liu, E. del Barco, S. Hill, *Phys. Rev. B* **2012**, *85*, 12406.

7 a) T. Glaser, M. Gerenkamp, R. Fröhlich, *Angew. Chem. Int. Ed.* **2002**, *41*, 3823–3825; b) T. Glaser, *Chem. Comm.* **2011**, *47*, 116–130.

8 a) H. C. Longuet-Higgins, *J. Chem. Phys.* **1950**, *18*, 265–274; b) H. M. McConnell, *J. Chem. Phys.* **1963**, *39*, 1910.

9 a) H. Iwamura, *Adv. Phys. Org. Chem.* **1991**, *26*, 179–253; b) T. Glaser, H. Theil, M. Heidemeier, *C.R. Chim.* **2008**, *11*, 1121–1136; c) T. Glaser, *Coord. Chem. Rev.* **2013**, *257*, 140–152.

10 V. A. Ung, S. M. Couchman, J. C. Jeffery, J. A. McCleverty, M. D. Ward, F. Totti, D. Gatteschi, *Inorg. Chem.* **1999**, *38*, 365–369.

11 B. J. Kennedy, K. S. Murray, *Inorg. Chem.* **1985**, *24*, 1552–1557.

12 T. Glaser, M. Heidemeier, T. Lügger, *J. Chem. Soc., Dalton Trans.* **2003**, 2381–2383.

13 a) T. Glaser, M. Heidemeier, S. Grimme, E. Bill, *Inorg. Chem.* **2004**, *43*, 5192–5194; b) T. Glaser, M. Heidemeier, J. B. H. Strautmann, H. Bögge, A. Stammler, E. Krickemeyer, R. Huenerbein, S. Grimme, E. Bothe, E. Bill, *Chem. Eur. J.* **2007**, *13*, 9191–9206; c) S. Walleck, H. Theil, M. Heidemeier, G. Heinze-Brückner, A. Stammler, H. Bögge, T. Glaser, *Inorg. Chim. Acta* **2010**, *363*, 4287–4294; d) B. Feldscher, A. Stammler, H. Bögge, T. Glaser, *Dalton Trans.* **2010**, *39*, 11675–11685; e) B. Feldscher, A. Stammler, H. Bögge, T. Glaser, *Polyhedron* **2011**, *30*, 3038–3047; f) C.-G. Freiherr von Richthofen, A. Stammler, H. Bögge, T. Glaser, *J. Org. Chem.* **2012**, *77*, 1435–1448.

14 a) T. Glaser, M. Heidemeier, R. Fröhlich, P. Hildebrandt, E. Bothe, E. Bill, *Inorg. Chem.* **2005**, *44*, 5467–5482; b) H. Theil, C.-G. Freiherr von Richthofen, A. Stammler, H. Bögge, T. Glaser, *Inorg. Chim. Acta* **2008**, *361*, 916–924.

15 C.-G. Freiherr von Richthofen, A. Stammler, H. Bögge, M. W. DeGroot, J. R. Long, T. Glaser, *Inorg. Chem.* **2009**, *48*, 10165–10176.

16 a) T. Glaser, M. Heidemeier, T. Weyhermüller, R.-D. Hoffmann, H. Rupp, P. Müller, *Angew. Chem. Int. Ed.* **2006**, *45*, 6033–6037; b) V. Hoeke, M. Heidemeier, E. Krickemeyer, A. Stammler, H. Bögge, J. Schnack, A. Postnikov, T. Glaser, *Inorg. Chem.* **2012**, *51*, 10929–10954.

17 a) T. Glaser, M. Heidemeier, E. Krickemeyer, H. Bögge, A. Stammler, R. Fröhlich, E. Bill, J. Schnack, *Inorg. Chem.* **2009**, *48*, 607–620; b) V. Hoeke, E. Krickemeyer, M.

Heidemeier, H. Theil, A. Stammler, H. Bögge, T. Weyhermüller, J. Schnack, T. Glaser, *Eur. J. Inorg. Chem.* **2013**, *2013*, 4398–4409.

18 E. Krickemeyer, V. Hoeke, A. Stammler, H. Bögge, J. Schnack, T. Glaser, *Z. Naturforsch.* **2010**, *65b*, 295–303.

19 V. Hoeke, A. Stammler, H. Bögge, J. Schnack, T. Glaser, *Inorg. Chem.* **2014**, *53*, 257–268.

20 a) V. Hoeke, K. Gieb, P. Müller, L. Ungur, L. F. Chibotaru, M. Heidemeier, E. Krickemeyer, A. Stammler, H. Bögge, C. Schröder, J. Schnack, T. Glaser, *Chem. Science* **2012**, *3*, 2868–2882; b) V. Hoeke, M. Heidemeier, E. Krickemeyer, A. Stammler, H. Bögge, J. Schnack, T. Glaser, *Dalton Trans.* **2012**, 12942–12959.

21 a) T. Glaser, M. Heidemeier, R. Fröhlich, *C.R. Chim.* **2007**, *10*, 71–78; b) C. Mukherjee, A. Stammler, H. Bögge, T. Glaser, *Inorg. Chem.* **2009**, *48*, 9476–9484; c) T. Glaser, M. Heidemeier, H. Theil, A. Stammler, H. Bögge, J. Schnack, *Dalton Trans.* **2010**, *39*, 192–199; d) E. Krickemeyer, Y. Kaiser, A. Stammler, H. Bögge, T. Glaser, *Z. Anorg. Allg. Chem.* **2013**, *639*, 1527–1533.

22 a) C. Mukherjee, A. Stammler, H. Bögge, T. Glaser, *Chem. Eur. J.* **2010**, *16*, 10137–10149; b) B. Feldscher, E. Krickemeyer, M. Moselage, H. Theil, V. Hoeke, Y. Kaiser, A. Stammler, H. Bögge, T. Glaser, *Sci. China: Chem.* **2012**, *55*, 951–966; c) C.-G. Freiherr von Richthofen, A. Stammler, H. Bögge, T. Glaser, *Eur. J. Inorg. Chem.* **2012**, *2012*, 5934–5952; d) C.-G. Freiherr von Richthofen, B. Feldscher, K.-A. Lippert, A. Stammler, H. Bögge, T. Glaser, *Z. Naturforsch.* **2013**, *68b*, 64–86.

23 G. M. Sheldrick, *SADABS*, 2008, University of Göttingen: Göttingen, Germany.

24 G. M. Sheldrick, *Acta Crystallogr.* **2008**, *A64*, 112–122.

25 a) A. L. Spek, *PLATON/SQUEEZE*, Bijvoet Center for Biomolecular Research, Utrecht University, Utrecht, The Netherlands; b) P. Sluis, A. L. Spek, *Acta Crystallogr.* **1990**, *A46*, 194.

26 L. Cavallo, H. Jacobsen, *Eur. J. Inorg. Chem.* **2003**, 892–902.

27 J. Kruszewski, T. M. Krygowski, *Tetrahedron Lett.* **1972**, *13*, 3839–3842.

28 a) V. I. Lebedev, D. N. Laikov, *Dokl. Akad. Nauk* **1999**, *366*, 741–745; b) J. Schnack, *Condens. Matter Phys.* **2009**, *12*, 323–330.

29 a) B. Feldscher, H. Theil, A. Stammler, H. Bögge, T. Glaser, *Inorg. Chem.* **2012**, *51*, 8652–8654; b) B. Feldscher, A. Stammler, H. Bögge, T. Glaser, *Eur. J. Inorg. Chem.* **2013**, 388–397; c) B. Feldscher, H. Theil, A. Stammler, H. Bögge, T. Glaser, *Dalton Trans.* **2014**, *43*, 4102–4114.